2015

Metabolic Characterization of MPNST Cell Lines

Christopher A. Waker
Wright State University

METABOLIC CHARACTERIZATION OF MPNST CELL LINES

A thesis submitted in partial fulfillment
of the requirement for the degree of
Master of Science

By

CHRISTOPHER ANDREW WAKER
B.S., The Ohio State University, 2013

2015
Wright State University

WRIGHT STATE UNIVERSITY

GRADUATE SCHOOL

DATE OF DEFENSE
5/26/2015

I HEREBY RECOMMEND THAT THE THESIS PREPARED UNDER MY SUPERVISION BY Christopher Andrew Waker ENTITLED Metabolic Characterization of MPNST Cell Lines BE ACCEPTED IN PARTIAL FULFILLMENT OF THE REQUIREMENT FOR THE DEGREE OF Master of Science.

Debra Mayes, Ph.D.
Thesis Director

Christopher Wyatt, Ph.D.
Interim Chair, Department
of Neuroscience, Cell Biology and Physiology

Committee on
Final Examination

Debra Mayes, Ph.D.

Robert Putnam, Ph.D.

Christopher Wyatt, Ph.D.

Robert Fyffe, Ph.D.
Vice President for Research and
Dean of Graduate School

ABSTRACT

Waker, Christopher Andrew. M.S., Department of Neuroscience, Cell Biology, and Physiology, Wright State University, 2014. Metabolic characterization of MPNST cell lines.

Malignant transformation is the process by which cells develop cancer properties. While many causes for malignant transformation are known (i.e. common genetic mutations and/or exposure to toxins or viruses), the basic requirements that allow a cell to stay alive with altered nutrient and energy requirements are just now being studied. In some tumor types malignant cells undergo changes that result in metabolic differences compared to normal cells. These can include defects in mitophagy resulting in an accumulation of dysfunctional mitochondria and/or a metabolic switch resulting in increased glycolysis, termed the Warburg effect. Increased tumor growth and metastasis have also been associated with mitochondrial DNA mutations in some tumor types. In this study, we characterized the mitochondrial function of malignant peripheral nerve sheath tumor (MPNST) cell lines commonly used to study malignant transformation in Neurofibromatosis Type I. We identified metabolic differences between NF1-wildtype (STS26T) and NF1-deficient (ST88-14, 90-8, and S462) MPNST cell lines by measuring extracellular acidification and oxygen consumption, mitochondrial respiration protein expression, and ROS levels. Similar to findings from other malignant tumors, all MPNST cell lines were more glycolytic compared to non-tumorigenic

normal human Schwann cells and surprisingly NF1-deficiency correlated with lower glycolytic and mitochondrial respiratory rate compared to wildtype MPNST. Mitochondrial respiratory rates and respiratory protein expression were significantly lower in the NF1-deficient MPNST cell lines when compared to NF1-wildtype MPNST cells. These findings demonstrate that neurofibromin affects glycolysis and mitochondrial respiration in malignant cells.

TABLE OF CONTENTS

Page

I. INTRODUCTION 1

NF1 and Malignant Peripheral Nerve Sheath Tumors 2

Cancer and Metabolism 8

ROS, Mitochondria, and Cancer 14

Rationale 17

Hypothesis 20

Summary 21

II. MATERIALS AND METHODS 22

Cell Culture 23

Immunofluorescence 24

Extracellular Flux Analysis 26

ROS Assay 36

Western Blot Analysis 40

Statistics 45

III. RESULTS 46

NHSC are a Pure Culture 47

NF1-deficient MPNST lines have lower Glycolytic Rates than NF1-WT 50

NF1-deficient MPNST have lower Mitochondrial Respiration than NF1-WT 54

NF1-deficient MPNST are less metabolic than NF1-WT 58

Differential MPNST cell line Electron Transport Chain Protein Expression 61

NF1-deficient MPNST have decreased Uncoupling 64

MPNST Cell Line ROS Originate from Mitochondria 67

IV. DISCUSSION 71

Future Experiments 80

V. REFERENCES 83

List of Figures

Figure Page

1. ERK/MAPK Pathway 7

2. Electron Transport Chain and Oxidative Phosphorylation 13

3. Extracellular Flux Analysis Experimental Setup 29

4. Glycolysis Stress Test 32

5. Mitochondria Stress Test 35

6. CM-H_2DCFDA ROS Assay 39

7. NHSC are a Pure Culture 49

8. NF1-deficient MPNST Lines Have lower Glycolytic Rates than NF1-WT 53

9. NF1-deficient MPNST have lower Mitochondrial Respiration than NF1-WT 57

10. NF1-deficient MPNST are less metabolic than NF1-WT 60

11. Differential Expression of ETC proteins in MPNST 63

12. NF1-deficient MPNST have decreased Proton Leak Activity and Expression 66

13. MPNST Cell Line ROS Originate from Mitochondria 70

ACKNOWLEDGEMENTS

I would like to thank my advisor, Dr. Debra Mayes, for her support and patience. She welcomed me into her new lab and shared her diverse experiences in science, exposing me to the reality of a research career. Additionally, I must thank Dr. Salim El-Amouri for his technical assistance, advice, and wisdom. His work ethic is something we should all aspire to achieve. Thank you to Cameron Smith and Adam Tokarsky for their assistance and support.

Thank you to my committee members, Dr. Christopher Wyatt and Dr. Robert Putnam, for their advice and guidance. Thanks to Dr. Lucile Wrenshall for allowing me to use her microplate reader and thanks to Dr. Nancy Ratner and Dr. Karen Cichowski for providing the MPNST cell lines. Thanks to the Department of Neuroscience, Cell Biology & Physiology for the opportunity to expand my research experience. Finally, I want to thank my parents, family, and friends for their unwavering support. The end is in sight… somewhere.

LIST OF ABBREVIATIONS

2-DG: 2-deoxy-D-glucose

90-8: NF1-deficient MPNST cell line

Complex I: NADH:ubiquinone oxidoreductase

Complex II: Succinate-coenzyme Q reductase

Complex III: Coenzyme Q - cytochrome c reductase

Complex IV: Cytochrome c oxidase

Complex V: ATP synthase

Cyto C: Cytochrome C

ECAR: Extracellular acidification rate

ETC: Electron transport chain

MPNST: Malignant peripheral nerve sheath tumors

NF1: Neurofibromin

NF-1: Neurofibromatosis type 1

NF1-WT: Neurofibromin wildtype

NHSC: Normal human Schwann cells

NO: Nitric oxide

NOS: Nitric oxide synthase

eNOS: endothelial nitric oxide synthase

nNOS: neuronal nitric oxide synthase

OCR: Oxygen consumption rate

Q: coenzyme Q

ROS: Reactive oxygen species

S462: NF1-deficient MPNST cell line

ST88-14: NF1-deficient MPNST cell line

STS26T: NF1-wildtype MPNST cell line

UCP: Uncoupling proteins

UCP2: Uncoupling protein 2

INTRODUCTION

NF1 AND MALIGNANT PERIPHERAL NERVE SHEATH TUMORS

Malignant peripheral nerve sheath tumors (MPNST) are highly aggressive, invasive sarcomas of the connective tissue that surrounds peripheral nerves. MPNST account for nearly 10% of all soft tissue sarcomas (Doorn et al., 1995, Grobmyer et al., 2008) and typically present as a painful, rapidly enlarging mass, often diagnosed at an advanced stage with distant metastases that have a poor prognosis (Anghileri et al., 2006; Ferner and Gutmann, 2002). There is a low rate of sporadic MPNST development in the general population (0.001%) (Ferner and Gutmann, 2002; Ducatman et al., 1986); however, the lifetime risk is 8 to 13% in patients with Neurofibromatosis Type 1 (NF1) (Evans et al., 2002). In fact, almost half of all MPNST are diagnosed in NF1 patients. NF1 is also an indicator for poor prognosis, suggesting that *NF1* loss in MPNST may augment the potential detriment of this tumor type to human life (Porter et al., 2009).

Neurofibromatosis type 1 or von Recklinghausen disease is an autosomal dominant disease that occurs in approximately 1/3000 live births (Friedman 1999). NF1 is associated with defective functionality or mutations in the *NF1* gene, which can occur sporadically or be inherited (Riccardi 2010; Staser et al., 2010; Jett and Friedman 2010; Parrinello and Lloyd 2009; McClatchey 2007). Located at 17q11.2, *NF1* is a large, highly mutated gene, encompassing more than 350 kb and containing 61 exons (Ledbetter et al., 1989; Cawthon et al., 1990; Marchuk et al., 1991). Pathological mutations are found across the entire *NF1* gene and range from single nucleotide substitutions to large deletions (Zenker 2011).

NF1 belongs to a class of developmental disorders commonly called "RASopathies". These disorders are caused by germline mutations in genes that encode protein component(s) of the Ras/MAPK pathway family (Zenker 2011; Tidyman et al. 2009). Neurofibromin is a GTPase activating protein that increases the rate of Ras-GTP hydrolysis, converting active Ras-GTP to inactive Ras-GDP (Ballester et al., 1990; Martin et al., 1990; Xu et al., 1990). Ras is a membrane bound G-protein involved in the activation of MAPK/ERK pathway. The MAPK/ERK pathway plays a critical role in cell proliferation, growth, and differentiation. Therefore, loss of neurofibromin, a ubiquitously expressed protein, will cause an aberrant increase in Ras signaling that results in a multiplicity of observed manifestations with varying degrees of severity. Figure 1 shows the MAPK/ERK signal transduction pathway. NF1 patients are susceptible to learning deficits, psychiatric disorders and cognitive dysfunctions, bone and skeletal malformations, and vascular problems in addition to the development of tumors (Thomas et al. 2006; Shilyansky et al., 2010; Hyman et al., 2006; Rosser et al., 2003; Krab et al., 2008; Lee and Stephenson 2007).

Although individuals with NF1 are prone to developing other cancers, including optic glioma, leukemia, and juvenile myelomonocytic leukemia (JMML), the most common neoplasm in individuals with NF1 are benign nerve sheath tumors of the peripheral nervous system, called neurofibromas. Neurofibromas are present in >99% of NF1 patients (Ferner et al., 2006). Neurofibromas are thought to originate from nonmyelinating Schwann cells but contain other cell types like fibroblasts and mast cells (Zheng et al., 2008, Serra et al., 2000). The dermal or

subcutaneous type can be disfiguring, painful, and sensitive to touch but are not known to become malignant. Plexiform neurofibromas are large, slow growing, diffuse neoplasms with a propensity to enwrap structures within the body, often involving multiple nerve fascicles, nerve branches, and blood vessels. As with dermal neurofibromas, the plexiform type can be disfiguring and painful, but may additionally lead to loss of sensation and weakness (Korf 1999). Both tumor types can be asymptomatic.

Plexiform neurofibromas are found in 50% of NF1 patients and have the potential to become a malignant peripheral nerve sheath tumor (MPNST) (Tonsgard et al., 1998). The five-year survival rate for an NF1 patient with a MPNST was half that of patients with a sporadic MPNST (21%) from the date of diagnosis – indicating that loss of the NF1 protein may play a role in the aggressiveness of these tumors (Evans et al., 2002). The increased incidence of MPNST in the NF1 population contributes to a higher mortality rate, with the average age of death for NF1 patients being 54.4 years, 15.6 years lower than the 70.1 years for the general population at the time of the study (Rasmussen et al., 2001). However, a more recent meta-analysis of MPNST outcomes found no significant difference between patients with or without a diagnosis of NF1. These findings could be confounded as *NF1* mutation or loss may be implicated in some sporadic MPNST (Kolberg et al., 2013). Neurofibromatosis Type I cannot be cured and current therapies treat only symptoms and complications. Surgical resection is the treatment option of choice due to a lack of effective chemotherapies for MPNST. MPNST resection involves

functional loss of a nerve(s) that can have severe health complications contingent upon tumor location and size.

FIGURE 1

Depiction of the Ras activated ERK/MAPK pathway.

Activation of Ras through the Ras-Raf-MEK-ERK pathway results in increased cellular proliferation, survival, and transformation. TRK = Tyrosine receptor kinase, GRB2 = Growth factor receptor-bound protein 2, SOS = son of sevenless, NF1 = neurofibromin

FIGURE 1

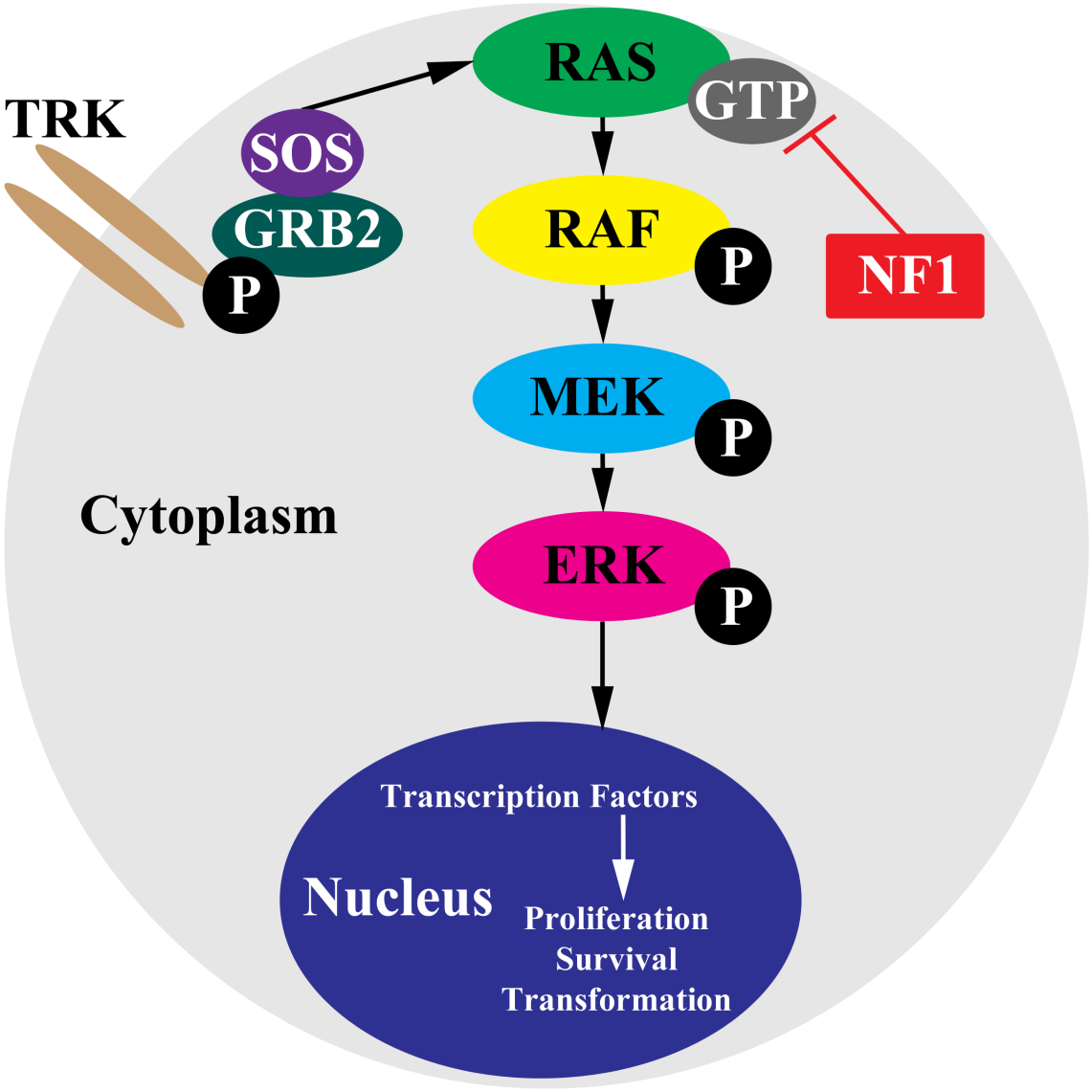
TRK
SOS
GRB2
P
RAS
GTP
RAF
P
NF1
MEK
P
Cytoplasm
ERK
P
Transcription Factors
Nucleus
Proliferation
Survival
Transformation

CANCER AND METABOLISM

Malignant transformation is the process by which cells acquire cancer properties and may occur in primary tissues or as a secondary transformation from a benign state. Malignant cells have accumulated genetic mutations that fundamentally alter cellular behavior. Some properties of cancer are: growth in the absence of growth factors, lack of contact inhibition, resistance to apoptosis and senescence, persistent telomerase activity, rapid growth, tissue invasion and metastases, clonal nature, and angiogenesis. Common genetic mutations, toxin exposure, and viruses are a few of the many known mutagens that cause malignant transformation. Metabolic changes also occur in malignant cells in response to the altered cellular behavior (Zhang and Yang, 2013).

Two of the major energy production pathways within cells are glycolysis and oxidative phosphorylation. Glycolysis is a serial process that consists of ten enzymatically catalyzed chemical reactions within the cytoplasm resulting in the degradation of glucose to pyruvate. ATP and electrons are produced as a consequence of glycolysis (Hill et al., 2012). Many of the intermediates generated in glycolysis serve as precursors in other biosynthetic pathways. The end product of glycolysis, pyruvate, is a regulatory modifier in multiple metabolic processes. For example, under normal oxygen conditions pyruvate can be funneled in the citric acid cycle, fermented to lactic acid in anoxic environments, and can also serve as a precursor for fatty acids and carbohydrates.

Increased glycolysis is often observed in cancer cells. This phenomenon has been well studied and is called the Warburg effect (Warburg, 1956). The Warburg

effect results in a glycolytic shift such that glucose consumption is increased. Because glucose consumption can be visualized and measured using fluorodeoxyglucose (FDG) positron emission tomography (PET), this technology is a common radiopharmaceutical imaging technique used in cancer diagnosis. Possible explanations for the Warburg effect (i.e. increased cellular glycolysis) include: 1) increased glycolytic biosynthetic precursor production necessary for tumor growth, 2) glycolysis can produce ATP at a faster rate than oxidative phosphorylation, and 3) a hypoxic microenvironment that will reduce cellular oxidative phosphorylation capabilities (Nakajima and van Houten, 2013).

Cancer cells construct more cellular components than normal cells because of increased proliferation. Pyruvate is used as a precursor for the synthesis of other molecules like fatty acids, cholesterol, and glucose that are involved in the construction of cellular components. Pyruvate can also feed into the citric acid cycle and pentose phosphate pathway, which in turn have intermediates that are precursors for amino acids, nucleotides, and tetrapyrroles (like the heme group in hemoglobin). Increased biosynthetic precursor production is essential for increased proliferation. Glycolysis is faster at producing energy than oxidative phosphorylation so rapidly dividing cells may utilize glycolysis more than oxidative phosphorylation because it can maintain pace with proliferation. Many tumors outgrow an adequate blood supply. Without sufficient blood perfusion, the oxygen supply is low, creating a hypoxic microenvironment. Many tumors are capable of increasing glycolysis to overcome this deprivation (Gillies et al., 2008). This forces

tumor cells to produce energy by anaerobic glycolysis as the capability of oxidative phosphorylation is diminished.

Oxidative phosphorylation, the other major energy production pathway, is far more efficient at ATP production than glycolysis. This process occurs in mitochondria. Mitochondria are often called the "powerhouse of the cell" as they produce most of the cell's energy. Oxidative phosphorylation utilizes electrons produced in glycolysis and the citric acid cycle to create a proton gradient across the inner-membrane of mitochondria (Hill et al., 2012). Protons are pumped out of the matrix and into the inter-membrane space by specialized proteins using the movement of electrons down the electron transport chain as energy. Electrons travel the transport chain towards increasing (higher) standard reduction potentials before reducing O_2 and forming water. The electrochemical proton gradient is used to power the production of ATP using ATP synthase (Complex V). In this process, protons follow their electrochemical gradient from the inter-membrane space into the matrix through ATP synthase. ATP synthase then mechanically forces ADP and Pi together producing ATP. Peter Mitchell first suggested the chemiosmotic theory of energy production in 1961 (Mitchell, 1961). Figure 2 is an illustration of the electron transport chain and oxidative phosphorylation.

Mitochondria have an important role in normal cellular homeostasis. Besides producing energy through oxidative phosphorylation, mitochondria also play an integral role in calcium storage and signaling, membrane potential regulation, apoptosis, steroid synthesis, and hormonal signaling. During malignant

transformation, mutations in the mitochondrial and nuclear DNA that influence these processes contribute to altered mitochondrial metabolism and signaling; however, the impact these changed mitochondria have on cells remains unclear. Recent evidence has demonstrated that some changes in the pathways that regulate metabolism and mitochondrial signaling can lead to tumorigenesis (Wallace, 2012).

FIGURE 2

Electron Transport Chain and Oxidative Phosphorylation

A depiction of the Chemiosmotic theory of energy production within mitochondria with the ETC and ATP synthase. ETC = electron transport chain, Complex I = NADH dehydrogenase, NADH = nicotimamide adenine dinucleotide, Complex II = succinate dehydrogenase, Q = coenzyme Q, Complex III = coenzyme Q-cytochrome C reductase, Cyto C = cytochrome C, Complex IV = cytochrome C oxidase, Complex V = ATP synthase, UCP = uncoupling protein

FIGURE 2

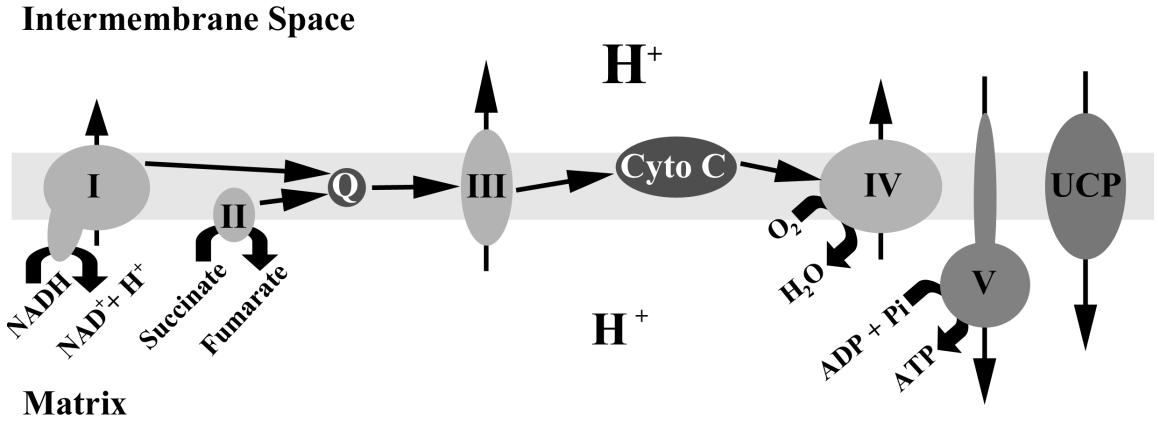
Intermembrane Space
H+
I
II
Q
III
Cyto C
IV
UCP
V
NADH
NAD+ + H+
Succinate
Fumarate
O2
H2O
ADP + Pi
ATP
H +
Matrix

ROS, MITOCHONDRIA, AND CANCER

A consequence of oxidative phosphorylation is the production of reactive oxygen species (ROS). ROS are a chemically reactive family of oxygen containing molecules that are involved in cellular signaling and the pathogen immune response. ROS like superoxides, peroxides, and hydroxyl radicals can cause cellular damage if allowed to accumulate – i.e. too much is being produced or too little is being neutralized. ROS can damage lipids, DNA, RNA, enzyme co-factors, and proteins by changing their chemical structure. The term, oxidative stress, describes the imbalance between the production of ROS and the cellular capability to neutralize it. Mitochondria are the largest producers of ROS in a cell. Increased ROS production is observed in tumor cells and is thought to contribute to tumorigenesis (Szatrowski et al., 1993). ROS are also known to regulate mitophagy and play a role in the glycolytic switch associated with the Warburg effect (Zhu et al., 2013 and Chen et al., 2015).

Autophagy or "self-eating" is the degradation of dysfunctional or unnecessary cellular components. The building blocks that make up the degraded cellular components may be recycled and used to build a different structure (Hill et al., 2012). A cell may use autophagy to maintain energy levels during starvation by deriving energy from the breakdown of cellular components. Autophagy has been well researched in cancer and the process has been shown to have both anti-tumor and tumor promoting capabilities for a cell (Boland et al., 2013). For example, autophagy can suppress cancer development through the degradation of damaged organelles and other cellular components, preventing the promotion of abnormal

proliferation and/or signaling. Alternatively, autophagy can promote tumor cell growth and survival by allowing the cell to compensate for metabolic stressors by using cellular components as an energy source. Metabolic stressors include: nutrient deprivation and excess, hypoxia, and oncogene activation (Wellen and Thompson, 2010).

Mitophagy is a mitochondria specific form of autophagy that is important in maintaining the appropriate amount of mitochondria in a cell. Every cell type has distinct energy requirements for optimal health and function. Therefore, mitochondrial content is a critical indicator for cell health. The amount of mitochondria within a cell is a tightly regulated balance between two processes: biogenesis and mitophagy. If the balance is disrupted resulting in too much or too little mitochondria then intracellular signaling and energy production can be thrown into disarray (Boland et al., 2013). Mitochondria are the major site of ROS production and are sensitive to oxidative damage. Damaged mitochondria may not produce ATP efficiently and may produce more ROS than healthy mitochondria, perturbing the balance between normal ROS production and ROS elimination. Mitophagy is a selective process that occurs to both healthy and damaged mitochondria. Mitophagy helps prevent the build-up of damaged mitochondria (Zhu et al., 2013).

Like autophagy, increased mitophagy has been observed in some cancers (Boland et al., 2013). Mitochondria increase ROS production in response to metabolic stress. Cells use mitochondrial ROS as an indicator of mitochondrial health (Wellen and Thompson, 2010). Moderate increases in ROS signal for

increased mitophagy as cellular function might be salvageable by elimination of the damaged mitochondria, while excessive increases in ROS signal apoptosis due to the probability of extensive systematic mitochondrial damage (Frank et al., 2012). Therefore, it makes sense that tumor cells would have an increase in ROS and mitophagy after episodes of oncogene activation, acidic or hypoxic tumor microenvironments and nutrient depletion. The increased glycolysis commonly found in tumors can result in an acidic tumor microenvironment, which is able to increase mitophagy through metabolic stress pathways. The same applies for the nutrient depletion that can occur when a tumor grows beyond the nutrient capability of its vascular supply. When a cell is not meeting its increased nutrient demands, it can start to degrade cellular components, including mitochondria. Growth beyond the vascular supply can also cause tissue hypoxia. Hypoxia can induce oxidative stress and promote mitophagy because not enough oxygen is present for proper mitochondrial respiration. The increased mitophagy/autophagy observed in some cancer cells lead to resistance to several classes of chemotherapeutic agents due to the more insular survival state of the tumor cell.

RATIONALE

Since the Ras/MAPK pathway family of proteins are known to regulate cell growth, and cellular proliferation necessitates specific energy requirements, it is particularly interesting to the NF1 tumorigenesis field that Ras and neurofibromin have been found to be localized in mitochondria (Roudebush et al., 1997, Amigoni et al., 2013). The purpose of NF1 and Ras in mitochondrial regulation is currently unknown. However, the probability that *NF1* loss in MPNST perpetuates a more aggressive tumor as NF1 patients with MPNST die at a faster rate than the general population, suggests that these pathways may play a role in the energy requirements necessary for tumor growth or transformation. Mitochondria play a vital role in balancing both energy regulation and a cell's response to stress – i.e. cellular life or death decisions. However, NF1-status dependent metabolic differences in malignant peripheral nerve sheath tumors have never been reported. Therefore, previous findings showing ROS-associated behavioral deficits with correlated mitochondria morphology alterations in murine models of *Nf1* loss or Ras hyperactivation, suggests that Nf1/Ras signaling pathway may influence mitochondrial heath and mitochondrial respiration (Mayes et al., 2013).

While metabolic changes in NF1 or MPNST have not been demonstrated, the effect of oncogenic Ras hyperactivation on metabolism has been studied. Increased glycolytic rates have been reported in hyperactive Ras or Ras transformed tumor cells, which is consistent with Warburg effect observations in many cancers (de Groof et al., 2009; Hu, Lu and Chen et al., 2012; Telang et al., 2006). However, data regarding the effect of Ras hyperactivation/transformation on mitochondrial

respiration is less consistent as both increases and decreases have been reported. A more recent report claimed that an increase in mitochondrial respiration during transformation precedes an ultimate decrease in the transformed cells (de Groof et al., 2009). Moreover, Ras transformed cells experience an "autophagy addiction", meaning that the transformed cells have increased autophagy that is required for tumorigenesis and to maintain some energy production via oxidative phosphorylation by ensuring a pool of healthy mitochondria (Guo, Chen, Mathew, and Fan et al., 2011).

MPNST cell lines have been used extensively throughout the years as an *in vitro* model for NF1. The goal of this study was to determine whether metabolic differences exist between MPNST cell lines and if neurofibromin plays a role. The MPNST cell lines in this study are primary cell lines derived from MPNST that occurred in patients. One cell line was derived from a cancer patient with no history or presentation of NF1 (STS26T) while the other three MPNST cell lines were derived from MPNST in NF1 patients (ST88-14, 90-8, and S462). The tumor lines are compared to each other and to normal human Schwann cells (NHSC). MPNST are thought to be tumors derived from a Schwann cell lineage but it has not been proven; therefore, these cells are probably the most appropriate non-tumorigenic control cell line at this time. We demonstrate for the first time that *NF1* status significantly affects the metabolic profiles of MPNST. *NF1* status correlates with differences in glycolysis and mitochondrial respiratory metabolic profiles and that the disparities in mitochondrial respiration might be partially attributable to changes in electron transport chain protein expression and decreased regulation of

oxidative phosphorylation by uncoupling proteins. A greater understanding of these metabolic differences may lead to a greater understanding of how the oncogene Ras transforms cells.

HYPOTHESES

1. MPNST cell lines will have a higher glycolytic rates than NHSC.

Many other tumors have shown higher glycolytic compared to non-tumorigenic cells, but these parameters have never been examined in MPNST sarcomas. We hypothesize that MPNST cell lines will have higher metabolic rates than normal human Schwann cells because they need to produce more energy to sustain increased growth rates.

2. NF1-patient derived MPNST cell lines will have lower mitochondrial respiration than sporadic (Ras not hyperactivated) MPNST

We hypothesize that NF1 patient derived MPNST cell lines will have decreased mitochondrial respiration because these cells should have a hyperactive Ras pathway. Ras hyperactivation may increase metabolic stress, giving rise to mitochondrial dysfunction and increased autophagy/mitophagy creating a lower mitochondrial content within the cells. In theory, tumor cells need more energy during transformation and therefore increase mitochondrial respiration. After tumor transformation, they shift their energy production in a Warburg effect (changing to become more glycolytic). We hypothesize that this shift will ultimately result in a new metabolic steady state with mitochondria content corresponding with reduced mitochondrial respiration.

SUMMARY

Malignant peripheral nerve sheath tumors currently have no effective chemotherapy. Half of all MPNST occur in the disease NF1. Mutations in neurofibromin, a negative regulator of the Ras oncogene, can lead to increased Ras signaling and cause NF1. Tumor cells often experience metabolic remodeling to a more glycolytic state in support an increased growth rate; the metabolic change ultimately depend on the energy requirements dictated by the oncogenic mutations. Ras transformed tumor cells experience increased mitochondrial dysfunction stemming from metabolic stress and increased mitophagy/autophagy among other possibilities. This study used Extracellular flux analysis, Western blot, immunocytochemistry, and ROS assays to characterize the metabolic profiles of common MPNST cell lines. We describe here how they differ from normal human Schwann cells and evaluate the role, if any, of neurofibromin loss on MPNST energy production.

MATERIALS AND METHODS

CELL CULTURE

The MPNST cell lines grew in DMEM/High Glucose Media (HyClone, Cat. No. SH30022.01) supplemented with 10% FBS (HyClone, Cat. No. SH30910.03), 1% Penicillin and Streptomycin (10,000 units/ml Penicillin and 10,000 units/ml Streptomycin, HyClone, Cat. No. SV30010), and 1% Amphotericin B (HyClone, Cat. No. SV30078.01). Primary normal human Schwann cells (NHSC) purchased from Creative Bioarray (Cat. No. CSC-7715W) grew in media provided by the supplier (Creative Bioarray, Cat. No. CSC-7715WM) supplemented with 1% Amphotericin B (HyClone, Cat. No. SV30078.01). The Schwann cell media formulation was 5% FBS, 1% Schwann cell growth serum, and 1% Penicillin and Streptomycin. All lines grew on cell culture treated, 55 cm^2 dishes (Corning, Cat. No. 430167). NHSC dishes were coated with 2.0 mg/cm^2 poly-L-lysine (Cultrex, Cat. No. 3438-100-01). Cell culture occurred in a Thermo Scientific 1300 Series A2, Class II biosafety cabinet employing aseptic technique. Cell lines were incubated in a humidified Thermo Scientific Forma Series II Water Jacket CO_2 Incubator at 37 °C and 7.5% CO_2/air (Yang and Ylipää et al., 2011). Cells were monitored closely and passaged upon reaching approximately 85% confluence using 0.05% trypsin-0.01% EDTA (Quality Biological, INC, Cat. No. 118-087-721). All cell lines were utilized in experiments before their 16^{th} passage.

IMMUNOFLUORESCENCE

The S100 protein family are normally expressed in cells derived from the neural crest and can be used as a marker for Schwann cells. S100 expression was used to determine the purity of the purchased normal human Schwann cells (NHSC). NHSC were seeded on CultureSlides at 2.0 $x10^5$ cells per well (BD Falcon, Ref No. 354108) coated with 2.0 $\mu g/cm^2$ poly-L-lysine (Cultrex, Cat. No. 3438-100-01). The slides incubated overnight in 7.5 % CO_2/air (Yang and Ylipää et al., 2011). Cells were washed (3x) with 1x PBS and fixed with 4% paraformaldehyde (Acros, 41678-5000) pH = 7.4 for 15 minutes. Slides were washed twice with cold 1x PBS and blocked for 1 hour using 10% normal goat serum (NGS) in 1x PBS. Cells were probed with anti-S100 antibody (Dako, Code No. Z 0311) at a 1:400 dilution in 10% NGS/PBS overnight at 4 °C. Slides were washed the next day (3x) and incubated with Rhodamine (TRITC)-conjugated Goat Anti-Rabbit secondary antibody (Jackson, Code No. 111-025003) at 1:100 dilution in 10% NGS/PBS for 1 hour at room temperature. Next the slides were stained with 4',6-diamidino-2-phenylindole (DAPI) (Thermo Scientific, No. 62248) at a 1:1000 dilution in PBS for 5 minutes at room temperature. Slides were washed (3x) with PBS and coverslipped using Fluoromount-G mounting media (SouthernBiotech, Cat. No. 0100-01). Images were taken using an Olympus BX51 Fluorescent Microscope and NIS Elements (Nikon) imaging software. TRITC was excited at 550 nm and emitted light at 570 nm, while DAPI was excited at 341 nm and emitted light at 452 nm. Analysis of the images

consisted of determining whether all nuclei stained with DAPI also stained with S100 protein.

Extracellular Flux Analysis

Extracellular acidification and oxygen consumption were monitored in live cells with an Extracellular Flux (XF) 24 Analyzer (Seahorse Bioscience, North Billerica, MA, USA). Extracellular acidification rate (ECAR) and oxygen consumption rate (OCR) are indicators of glycolysis and mitochondrial respiration. The Analyzer used fluorophores that change emission intensity in response to oxygen and pH levels in the extracellular space. The rates were normalized to the number of cells plated. Figure 3 shows the Extracellular Flux Analysis experimental set up.

Cells were liberated from dishes with 0.05% trypsin-0.01% EDTA solution (Quality Biological, INC, Cat. No. 118-087721) and counted using a dye exclusion method utilizing Trypan blue solution (HyClone, Cat. No. SV30084.01). Solubilized cells were diluted to 10x the desired density and were seeded in 100 µl of growth media on Seahorse Bioscience V7 plates (Part No. 100777-004) coated with 2.0 µg/cm^2 poly-L-lysine (Cultrex, Cat. No. 3438-100-01) for NHSC or 1.6 µg/cm^2 mouse laminin (Corning, Cat. No. 354232) for MPNST cell lines. The STS26T, 90-8, S462 were seeded at 4.0 x10^5 cells per well, while NHSC and ST88-14 cell lines were seeded at 8.0 x10^5 cells per well. Seeding number was established by cellular morphology and drug response, following the manufacturer's direction (data not shown). To prevent edge-effects, a two step seed method was employed; seeded plates remained in the hood at room temperature for 1 hour before being moved to the incubator for 1 hour. After resting, 150 µl of growth media was added to each

well. The plates were incubated overnight in 7.5% CO_2/air at 37 °C (Yang and Ylipää et al., 2011).

The XF24 Extracellular Flux analyzer sensor cartridge was hydrated with 1 ml of calibrant (Seahorse Bioscience, Part No. 100840-000) per well and allowed to incubate overnight in ambient air at 37 °C. Reconstitution of the XF Glycolysis Stress Test Kit (Seahorse Bioscience, Part No. 103015-100) and XF Mito Stress Test Kit (Seahorse Bioscience, Part No. 101706-100) followed manufacturer directions.

In these experiments, growth media was replaced with 525 µl assay media. Glycolysis Stress Test assay media consisted of unbuffered XF Base Medium Minimal DMEM (Seahorse Bioscience, Part No.102353-100) supplemented with 2.5 mM L-glutamine (Hyclone, Cat. No. SH30034.02). While the Mitochondrial Stress Test assay media was comprised of unbuffered XF Base Medium Minimal DMEM supplemented with 2.5 mM L-glutamine, 2.0 mM sodium pyruvate (Sigma Life Science, S8636) and 25.0 mM D-glucose (Sigma Life Science, Cat. No. G7528-250G). The D-glucose concentration (25.0 mM) was used in the stress test assay media because the same concentration was present in the cell lines' normal growth media. XF Base Medium Minimal DMEM does not natively contain D-glucose. Assay media was adjusted to pH = 7.35 ± 0.05 at 37 °C and filtered using 0.2 µm pore disposable filter units (Thermo Scientific, Cat. No. 09-741-04). The cells incubated for 1 hour in assay media in a CO_2-free incubator to deplete bicarbonate buffering before analysis. Stress Tests used mix/wait/measure times of 3/0/3 min, 75 µl drug injections, and took 3 measurements after each condition change. All experiments were conducted at 37 °C in ambient air.

FIGURE 3

XF24 Extracellular Flux Analyzer Experimental Setup

Attached to the probes on the sensor cartridge are two fluorophore dots that respond to changes in extracellular pH and oxygen. Drugs are injected pneumatically by a puff of air. The Extracellular Flux Analyzer calculates rates of extracellular flux for protons (pH) and oxygen. Image used with permission from Seahorse Bioscience (North Billerica, MA).

FIGURE 3

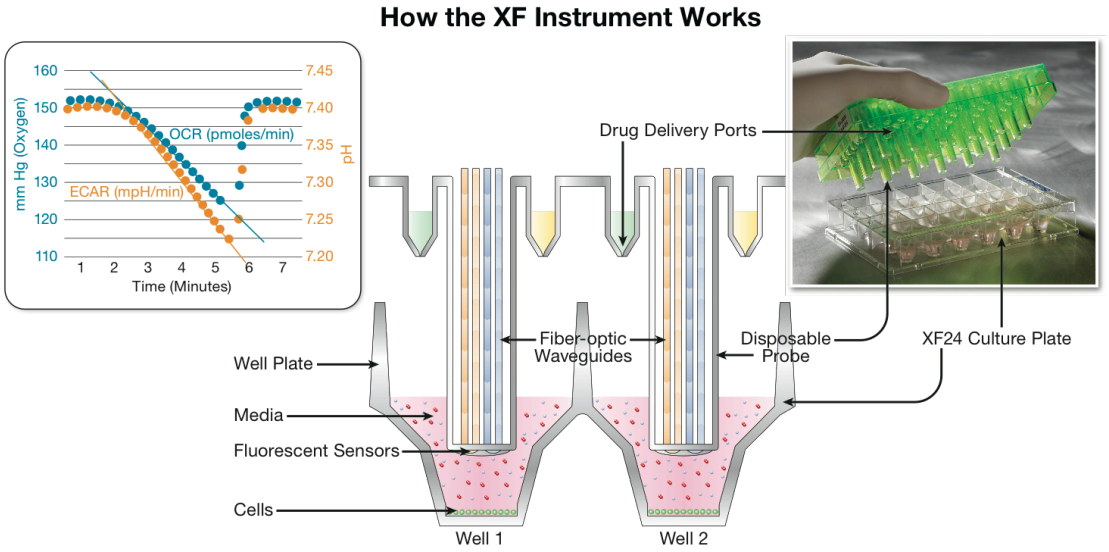
How the XF Instrument Works
160
150
140
130
120
110
mm Hg (Oxygen)
7.45
7.40
7.35
7.30
7.25
7.20
pH
OCR (pmoles/min)
ECAR (mpH/min)
1 2 3 4 5 6 7
Time (Minutes)
Drug Delivery Ports
Fiber-optic Waveguides
Disposable Probe
XF24 Culture Plate
Well Plate
Media
Fluorescent Sensors
Cells
Well 1
Well 2

GLYCOLYSIS STRESS TEST

The XF24 analyzes the extracellular change in pH and calculates a rate for each time point. The change in pH is a product of and therefore directly related to glycolytic flux. The Glycolytic profile for each cell line comes from rate differences between specific times in the course of the experiment. Figure 4 shows a generalized Glycolysis Stress Test and provides general relationships between the Glycolytic profile components and the rate data output. Initial extracellular acidification rates was measured in media without glucose then 10.0 mM Glucose was injected and the ECAR increased in response to the increased utilization of glucose by glycolysis and production of lactic acid. Oligomycin A (1 μM) was added next. Oligomycin A inhibits Complex V (ATP synthase) resulting in increased glycolysis (and therefore proton production and excretion) to satisfy the cellular energy needs no longer being met by oxidative phosphorylation. 2-deoxy-D-glucose (2-DG) was added last and competitively inhibits hexokinase, the enzyme catalyzing the first step of glucose degradation in glycolysis. The 100 mM 2-DG concentration used in the assay ensures complete hexokinase saturation allowing the ascription of ECAR measured after 2-DG addition to other proton producing processes besides glycolysis. The Glycolysis Stress Test assay data values are comprised of the following groups: NHSC (n=7), STS26T (n=10), ST88-14 (n=6), 90-8 (n=5), and S462 (n=5).

FIGURE 4

Glycolysis Stress Test

A general Glycolysis Stress Test output, the picture demonstrates the relationship between Glycolytic Profile parameters. Oligomycin (A) = inhibits ATP synthase, 2-deoxy-D-glucose (2-DG) = inhibits hexokinase

FIGURE 4

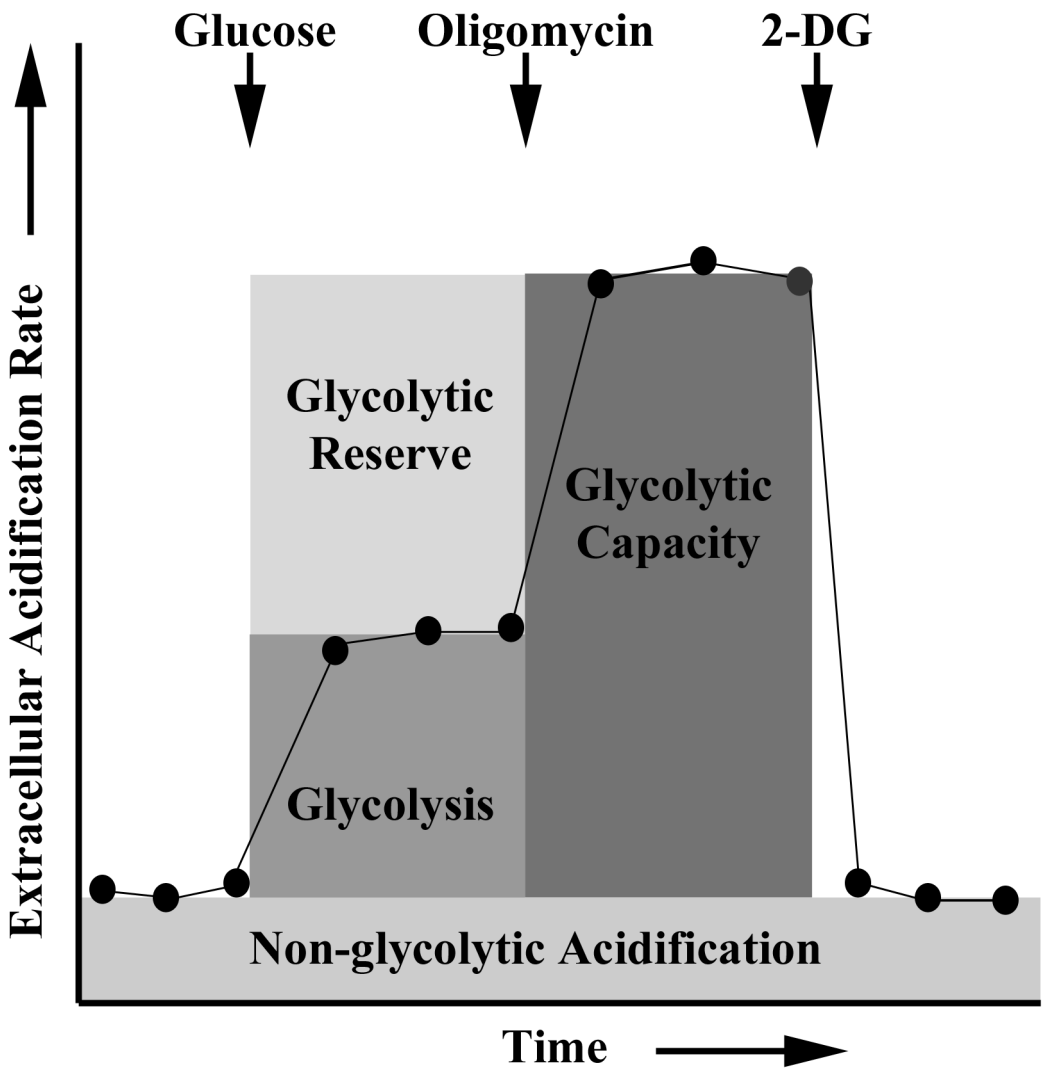
Glucose
Oligomycin
2-DG
Extracellular Acidification Rate
Glycolytic Reserve
Glycolytic Capacity
Glycolysis
Non-glycolytic Acidification
Time

MITOCHONDRIAL STRESS TEST

The Mito Stress Test measures the consumption of oxygen from the extracellular space. Oxygen is the final electron acceptor in the electron transport chain and is a good measure of mitochondrial respiratory activity. The Mito Stress Test used sequential injections of 1.0 μM Oligomycin A, 1.0 μM carbonyl cyanide 4-(trifluoromethoxy)phenylhydrazone (FCCP), and 1.0 μM Rotenone and Antimycin A to assess mitochondrial function. Basal Respiration was measured before drug addition and is the normal rate of oxygen consumption for the cells. Oligomycin A was injected first and inhibits Complex V (ATP Synthase). OCR decreased because the only oxygen being consumed to sustain the proton electrochemical gradient was in support of proton leak. The next drug added was FCCP–an ionophore that acts as a proton channel, providing protons a route across lipid bilayers. FCCP dissipated the proton gradient driving ATP synthase mediated ATP production and proton leak. The gradient dissolution uncouples the electron transport chain from ATP synthesis and allows the electron transport chain (Complexes I, II, III, and IV) to work at the maximal rate. Rotenone and Antimycin A were added last and simultaneously. Rotenone and Antimycin A inhibit Complexes I and III, respectively. The inhibition of Complex I and III shut down the electron transport chain and remaining OCR measured is attributed to processes other than mitochondrial respiration. Mitochondrial Stress Test assay data are comprised of the following groups: NHSC (n=7), STS26T (n=10), ST88-14 (n=6), 90-8 (n=5), and S462 (n=10).

FIGURE 5

Mitochondria Stress Test

A general Mitochondrial Stress Test that demonstrates the relationships between Mitochondrial Metabolic Profile parameters. Oligomycin (A) = inhibits ATP synthase (Complex V), FCCP = dissipates electrochemical proton gradient, Rotenone = inhibits Complex I, Antimycin A = inhibits Complex III

FIGURE 5

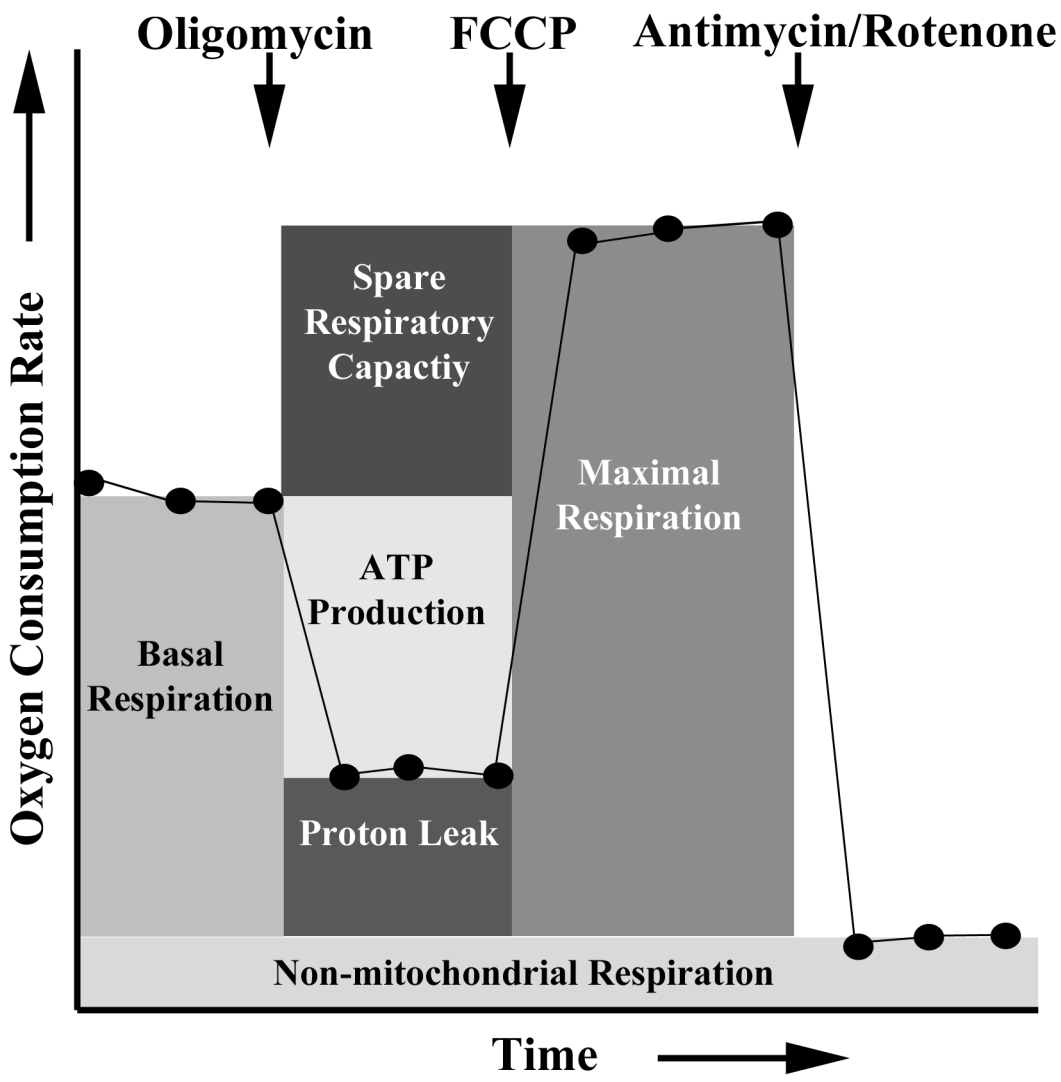
Oligomycin
FCCP
Antimycin/Rotenone
Oxygen Consumption Rate
Spare Respiratory Capactiy
Maximal Respiration
ATP Production
Basal Respiration
Proton Leak
Non-mitochondrial Respiration
Time

REACTIVE OXYGEN SPECIES ASSAY

STS26T, 90-8, S462 were seeded at 4.0 x10^5 cells per well, while NHSC and ST88-14 cell lines were seeded at 8.0 x10^5 cells per well of a 96-well plate (Falcon, REF: 353072) coated with 2.0 μg/cm^2 poly-L-lysine (Cultrex, Cat. No. 3438- 100-01) for NHSC or 1.6 μg/cm^2 mouse laminin (Corning, Cat. No. 354232) for MPNST cell lines. Cell lines were plated at different densities to mirror the Extracellular Flux Analyzer experimental set up. The cells incubated overnight at 37 °C at 7.5% CO_2/air in phenol red free DMEM/High Glucose (HyClone, Cat. No. SH30284.01) supplemented with 1% FBS (HyClone, Cat. No. SH30910.03), 1% Penicillin and Streptomycin (HyClone, Cat. No. SV30010), and 1% Amphotericin B (HyClone, Cat. No. SV30078.01).

Cells were washed the next day with 1x PBS and incubated in 8.65 mM 5-(and-6)-chloromethyl-2′,7′-dichlorodihydrofluorescein diacetate, acetyl ester (CM-H_2DCFDA) (Invitrogen Molecular Probes, Cat. No. C6827) dissolved in 1x PBS for 30 minutes. As the compounds are liable to undergo photo-oxidation, care was taken to limit exposure to light. Cells were washed with 1x PBS (2x 200ml) and allowed to recover in the incubator with 300 ml of phenol red free DMEM/High Glucose for 30 minutes. Fluorescence was measured using a BioTek Synergy H1 Multi-Mode Reader with excitation at 495 nm and emission at 527 nm. The well intensities were normalized to the seed density for each cell line, and then divided by the average intensity for NHSC. The background fluorescence was taken into account for each

cell line and results are reported as average fold change in ROS from NHSC ± standard error of the mean. The Reactive Oxygen Species Assay groups were n=8.

CM-H_2DCFDA is non-fluorescent and possesses two acetate groups that decrease the polarity of the compound allowing it to easily pass through lipid bilayers, once inside the cell endogenous esterases cleave the acetates, activating the chemical. The compound also contains chloromethyl groups that react with intracellular thiols supposedly increasing the retention of the compound within the cell compared to other chemical derivatives. The inactive molecules are oxidized by reactive oxygen species creating a fluorescent compound. Excitation of the fluorescent compound allows the electrons to jump to higher energy orbital that will then emit light when they decay back down to a lower energy orbital. Figure 6 exhibits the probable CM-H_2DCFDA mechanism of action.

FIGURE 6

CM-H_2DCFDA ROS Assay

A schematic that details a possible mechanism of action for the CM-H_2DCFDA determination of ROS levels. CM-H_2DCFDA = 5-(and-6)-chloromethyl-2′,7′-dichlorodihydrofluorescein diacetate, acetyl ester

FIGURE 6

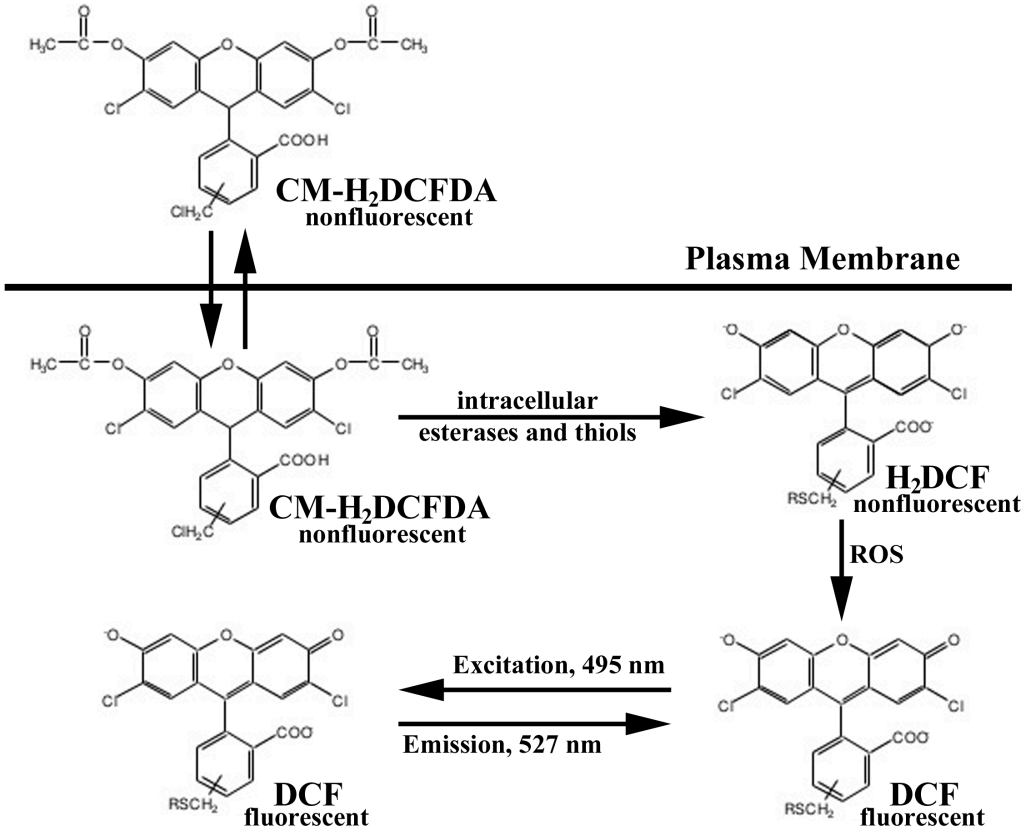
CM-H2DCFDA
nonfluorescent
Plasma Membrane
intracellular
esterases and thiols
CM-H2DCFDA
nonfluorescent
H2DCF
nonfluorescent
ROS
Excitation, 495 nm
Emission, 527 nm
DCF
fluorescent
DCF
fluorescent

WESTERN BLOT ANALYSIS

PROTEIN COLLECTION

Cells (1.3 x10^6 per well) were seeded on a 6-well plate (Falcon, Ref. 353046) coated with 2.0 μg/cm^2 poly-L-lysine (Cultrex, Cat. No. 3438-100-01) for NHSC or 1.6 μg/cm^2 mouse laminin (Corning, Cat. No. 354232) for MPNST. The cells incubated overnight in their respective growth media and protein lysate was collected the following day. While on ice, the cells were washed with 1x PBS (3x 1ml) then 300 ml Lysis Buffer (25 mM Tris-HCl, pH 7.4, 150 mM NaCl, 0.1 % SDS, 1 % Triton X-100, and 1% deoxycholate) was added to each well. Cells were manually scraped off the plate and triturated for 30 seconds until all visible occlusions had broken apart. The solution was transferred to the 1.5 ml tubes on ice and spun at 4 °C, 1 x10^5 rpm for 5 minutes (Eppendorf, Centrifuge 5424 R). The supernatant was transferred to fresh 1.5 ml tubes.

PROTEIN QUANTIFICATION

Protein concentration was measured using the colorimetric Pierce BCA Protein Assay Kit (Thermo Scientific, Prod. No. 23227). The BCA Protein Assay Kit uses a variation of the biuret reaction in which Cu^{2+} reduces to Cu^{1+} in the presence of protein and is then chelated by bicinchoninic acid (BCA) (Smith, et al 1985). Two BCA molecules combine with one Cu^{1+} resulting in a purple product with an absorbance at 562 nm. A sample of each protein lysate was diluted 1:10 in double distilled water. The sample to working reagent ratio was 1:20 for a total volume of

200 ml. The 96-well plate was shaken for 30 sec at 200 rpm (Benchmark, Incu-Shaker 10L) and then incubated for 30 min at 37 °C. The plate cooled to room temperature and the absorbance was measured using a BioTek Synergy H1 Multi-Mode Reader at 562 nm. Each absorbance value was an average of two measurements minus the average of two blanks. A linear curve of best fit modeled the Beer's Law relationship.

GEL ELECTROPHORESIS

Gel electrophoresis separates proteins by size with smaller proteins running faster than bigger ones. A 12% resolving gel was made using Acrylamide/Bis (29:1) 30% Solution (4 ml, Hoefer, GR329-500), 1.5 M Tris-HCL with pH = 8.8 (2.5 ml), 10% SDS-ddH_2O (0.1 ml), ddH_2O (3.35 ml), 10% ammonium persulfate (50 ml), and Tetramethylethylenediamine (5 μl TEMED). The glass plates were washed with 70% ethanol-ddH_2O before clamped into place and checked for leaks.

Volume of lysate equal to 20 μg of protein was added to 1.5 ml tubes with the appropriate volume of 6x Laemmli SDS Sample Buffer (Bioworld, Cat. No. 10570019-2) to dilute it to 1x and 10% (v/v) b-mercaptoethanol (Acros Organics, Code: 125472500). The tubes were boiled at 95 °C (Benchmark myBlock) for 5 minutes, spun for 30 seconds (BioExcell MiniFuge), and placed on ice to cool. The sodium dodecyl sulfate (SDS) gel lanes were loaded with the 20 μg of protein. Protein ladder (10 μl, Amersham, Prod. Code: RPN800E) was loaded and later used to determine relative protein size. The gel was run at 100V for 90 minutes in 1x SDS

Running Buffer. Stock 10x SDS Running Buffer is comprised of 0.25 M Tris Base (Fisher Scientific, BP152-10), 1.92 M Glycine (Fisher Scientific, BP381-5), and 35 mM SDS (Fisher Scientific, BP166-500) in double distilled water.

MEMBRANE TRANSFER

After separation, proteins were transferred to a more stable membrane. Foam, paper and 0.2 μm nitrocellulose membrane (Bio-Rad, 162-0112) were soaked in 1x Transfer Buffer for 5 minutes. Stock 10x Transfer Buffer is made of 250 mM Tris Base (Fisher Scientific, BP152-10) and 1.92 M Glycine (Fisher Scientific, BP381-5) in double distilled water. 1x Transfer Buffer is made from 800 ml of 10x Transfer Buffer, 1600 mL methanol (Fisher Scientific, BP1105-4), and 5.6 L double distilled water. Each layer was wetted with 1x Transfer Buffer as they were layered with caution to avoid bubbles. Transfer ran at 100V for 1 hour with ice surrounding the entire apparatus to keep the process cool limiting gel degradation.

DETECTION

The membrane was blocked with 5% (w/v) non-fat dry milk (Kroger Brand) in TBST (20 mM Tris HCl (Fisher Scientific, BP153-500) pH = 7.5, 150 mM NaCl, 0.05% (v/v) Tween 20 (Fisher Scientific, BP337-500) in double distilled water) for 1 hour at room temperature. The membrane was probed with primary antibody in 2% (w/v) of non-fat dry milk in TBST overnight at 4 °C or 1 hour at room temperature. The primary antibodies used are as follows: anti-Complex I subunit

NDUFB8 mouse monoclonal (Invitrogen Molecular Probes, Cat. No. 459210) in a 1:1000 dilution, anti-Cytochrome C rabbit monoclonal (Abcam, Cat. No. 04-1043), anti-Complex IV subunit IV mouse monoclonal antibody (Invitrogen Molecular Probes, Cat. No. A21347) in a 1:1000 dilution, anti-Complex V (ATP Synthase) subunit alpha mouse monoclonal antibody (Invitrogen Molecular Probes, Cat. No. 459240) in a 1:1000 dilution, anti-UCP2 (G-6) mouse monoclonal antibody (Santa Cruz Biotechnology, sc-390189) in a 1:500 dilution, anti-nNOS rabbit monoclonal antibody (Cell Signaling, #4231) in a 1:1000 dilution, and anti-eNOS rabbit monoclonal antibody (Cell Signaling, #9586) in a 1:1000 dilution.

The membranes were washed the next morning with TBST (3x 10 ml) to remove unbound primary antibody, then were probed for 1 hour at room temperature with the secondary antibody in 2% (w/v) non-fat dry milk/TBST. The secondary antibodies used were: HRP-conjugated anti-mouse IgG (Cell Signaling Technology, #7076) in a 1:3000 dilution and HRP-conjugated anti-rabbit IgG (Cell Signaling, #7074) in a 1:1000 dilution. Unbound secondary was washed out with TBST (3x 10 ml) followed by PBS (1x 10 ml). The purpose of the secondary antibody is to increase the resolution of the technique by forcing a second round of selection on the protein of interest.

The detection process uses a combination of two reagents, luminol and hydrogen peroxide, and the HRP conjugated to the secondary antibody. Immobilon Western Chemiluminescent HRP substrate (Millipore, Cat. No. WBKLS0500) was mixed in a 1:1 ratio and applied to the membrane for about 2 minutes. Hydrogen peroxide is cleaved by HRP into an unstable and highly reactive hydroxyl radical

that reacts with luminol creating a high energy intermediate. The high energy intermediate emits blue visible light as the high energy electron decays to a lower energy orbital. The light given off was detected by blue autoradiophrahy film (WorldWide Medical Products, Inc., BioExcell, 41101002). Film was processed using a Konica Minolta SRX-101A Medical Film Processor.

Even protein loading was determined by comparing levels of β–actin. Remaining ECL was washed out with TBST (2x 10 ml) and the membrane was stripped for 15 minutes with Restore Western Blot Stripping Buffer (Thermo Scientific, Prod. # 21059). The stripping buffer was washed out using TBST 3x 10 minutes and the membrane was blocked with 5% non-fat dry milk in TBST for 1 hour. The membrane was probed with β-actin rabbit monoclonal antibody conjugated with horseradish peroxidase (HRP) (Cell Signaling Technology, #5125) in a 1:4000 dilution in 2% non-fat dry milk TBST overnight at 4 °C or at room temperature for 1 hour. Excess antibody was washed out with TBST (3x 10 ml) and ECL was applied and film was re-exposed.

Relative protein expression levels were calculated by dividing each MPNST band densitometry measurement by the NHSC densitometry measurement for each protein probed. The band densitometries were calculated using Image Studio Lite Version 4.0.

STATISTICS

Values represented as mean ± standard error of the mean. Data was analyzed using Microsoft Excel 2011. Figures were made with Photoshop Elements 12 Editor. One-way ANOVA with Tukey post hoc was calculated using Prism 3.03. P-values less than 0.05 were considered statistically significant.

RESULTS

NORMAL HUMAN SCHWANN CELLS ARE A PURE CULTURE

S100 is a family of proteins that contain calcium-binding sites and are normally found in cells derived from the neural crest. S100 expression is used as a marker for Schwann cells. Normal human Schwann cells purchased from Creative Bioarray were probed for S100 expression, and counterstained with DAPI. DAPI is a nuclear marker. The finding that all DAPI stained nuclei also stained for S100 indicates that the NHSC were not contaminated with other cell types like fibroblasts and are a pure culture. Figure 7 contains representative images of NHSC stained with S100 and DAPI.

FIGURE 7

NHSC are a Pure Culture

S100 protein is used as a marker of Schwann Cells. DAPI is a nuclear stain. All nuclei co-localized with S100 staining indicating that the normal human Schwann cell line used is not contaminated with other cell types and is a pure Schwann cell culture. Images shown are representative.

FIGURE 7

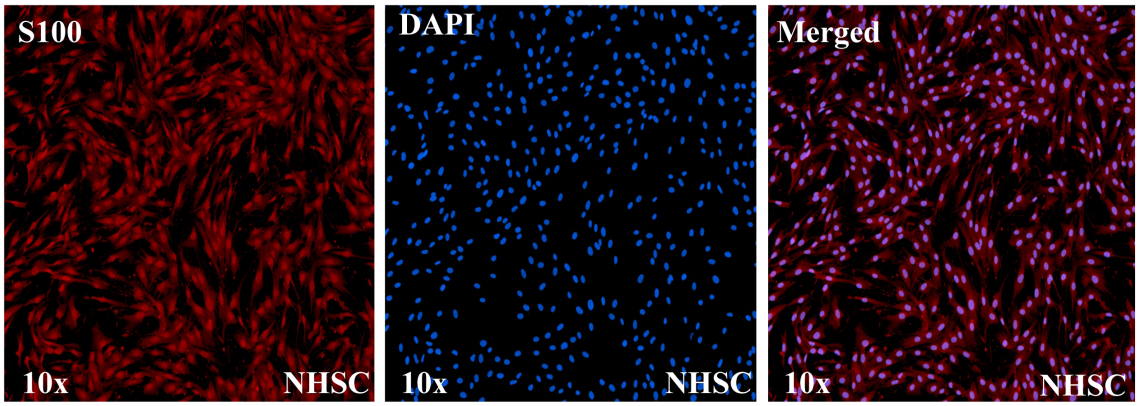

NF1-DEFICIENT MPNST LINES HAVE LOWER GLYCOLYTIC RATES THAN NF1-WILDTYPE

To determine whether NF1 plays a role in metabolism several different cell lines were submitted to metabolic stressors. The STS26T has been used extensively as the NF1-wildtype MPNST line. The presence of neurofibromin was confirmed in STS26T (Mattingly et al., 2006). The ST88-14, 90-8, and S462 lines are derived from NF1 patient MPNST and are used to model neurofibromin deficient cells (Patel et al., 2012; Wu et al., 2014). Figure 8B contains the extracellular acidification rates (ECAR) outputs for these cell lines.

Glycolysis ECAR (Figure 8C) was investigated first using D-glucose. Glycolytic rate is important to human MPNST outcomes because the tumors are commonly monitored and graded using FDG positron emission tomography. The Glycolysis extracellular acidification rates (mean ± SEM) in μpH/min/cell are: 0.14 ± 0.02 for NHSC, 0.77 ± 0.07 for STS26T, 0.24 ± 0.01 for ST88-14, 0.30 ± 0.03 for 90-8, 0.62 ± 0.02 for S462 (Figure 8C). All MPNST cell lines have significantly faster glycolytic rates than NHSC except for ST88-14, which was higher but not significantly so. STS26T were significantly higher than all other lines while S462 were significantly different from all other lines.

The second parameter explored was Glycolytic Capacity (Figure 8D) using Oligomycin A and D-glucose. The Glycolytic Capacity approaches the maximum glycolytic potential following ATP synthase inhibition. Glycolytic Capacity demonstrates the glycolytic rate required to meet all cellular energy requirements

and is important to cancer metabolism because it indicates how energetic transformed cells are and how glycolytic they could be. The Glycolytic Capacity ECAR (mean ± SEM) in μpH/min/cell are: 0.40 ± 0.04 for NHSC, 1.95 ± 0.10 for STS26T, 0.59 ± 0.01 for ST88-14, 0.76 ± 0.06 for 90-8, and 1.24 ± 0.04 for S462 (Figure 8D). All MPNST cells lines have a significantly higher Glycolytic Capacity than NHSC with the exception of ST88-14, which was higher but not significantly so. The NF1-wildtype MPNST line's (STS26T) Glycolytic Capacity was significantly higher than the other lines. NF1-deficient MPNST cell lines were significant lower than NF1-wildtype MPNST. The 90-8 line was significantly different from all others except for ST88-14. S462 were significantly different from all other cell lines.

Glycolytic Reserve (Figure 8E) shows the glycolytic rate increase required to match the energy output by mitochondrial respiration. Glycolytic Reserve can be used as evidence for glycolytic or mitochondrial respiratory protein activity differences. Glycolytic Reserve was tested using D-glucose and Oligomycin A. The Glycolytic Reserve ECAR (mean ± SEM) in μpH/min/cell are: 0.26 ± 0.05 for NHSC, 1.18 ± 0.12 for STS26T, 0.35 ± 0.02 for ST88-14, 0.45 ± 0.07 for 90-8, and 0.61 ± 0.05 for S462 (Figure 8E). The NF1-deficient MPNST cell lines were significantly lower than the NF1-wildtpye MPNST; the STS26T line was significantly higher than all other cell lines. All MPNST cell lines have significantly different Glycolytic Reserves except for ST88-14 and 90-8. ST88-14 was not significantly different from NHSC and 90-8. Glycolytic Reserve differences are probably due to variation in protein expression or activity levels.

FIGURE 8

NF1-DEFICIENT MPNST LINES HAVE LOWER GLYCOLYTIC RATES THAN NF1-WILDTYPE

(A) Representative depiction of Glycolytic Stress Test. (B) Glycolytic Stress Test for NHSC and MPNST lines. NHSC and STS26T are NF1-wildtype. ST88-14, 90-8, and S462 are NF1-deficient. (C) Glycolytic rate (D) Glycolytic Capacity (E) Glycolytic Reserve. Results are mean ± SEM. n = 5-10. P values determined by one-way ANOVA with Tukey post hoc. NHSC = Normal Human Schwann Cells, 2-deoxy-D-glucose (2-DG) = inhibits hexokinase

FIGURE 8

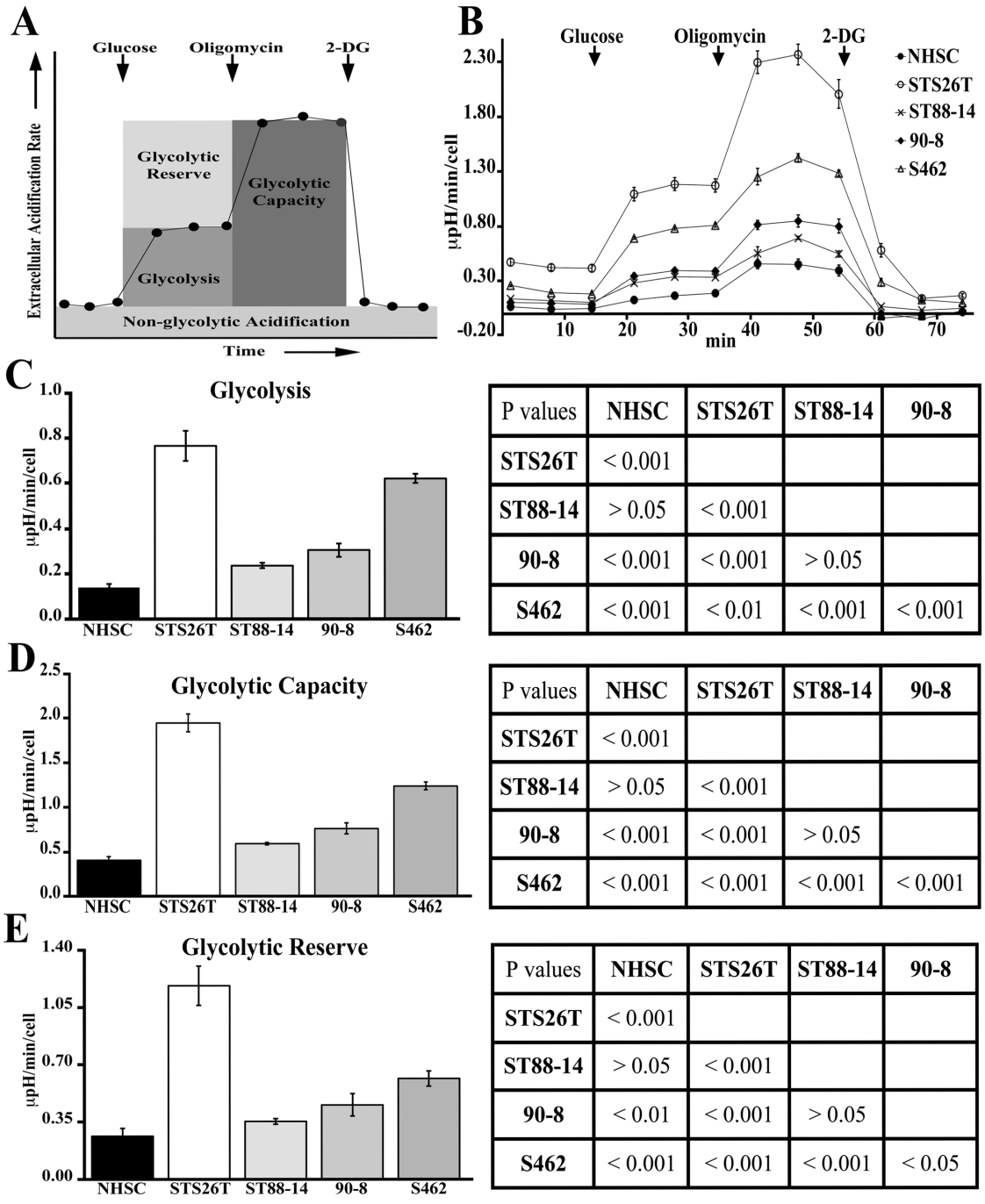

P values	NHSC	STS26T	ST88-14	90-8
STS26T	< 0.001			
ST88-14	> 0.05	< 0.001		
90-8	< 0.001	< 0.001	> 0.05	
S462	< 0.001	< 0.01	< 0.001	< 0.001

P values	NHSC	STS26T	ST88-14	90-8
STS26T	< 0.001			
ST88-14	> 0.05	< 0.001		
90-8	< 0.001	< 0.001	> 0.05	
S462	< 0.001	< 0.001	< 0.001	< 0.001

P values	NHSC	STS26T	ST88-14	90-8
STS26T	< 0.001			
ST88-14	> 0.05	< 0.001		
90-8	< 0.01	< 0.001	> 0.05	
S462	< 0.001	< 0.001	< 0.001	< 0.05

NF1-DEFICIENT MPNST HAVE LOWER MITOCHONDRIAL RESPIRATION THAN NF1-WILDTYPE

To evaluate whether NF1 status has a role in tumor oxidative phosphorylation MPNST cell lines with and without functional *NF1* were submitted to metabolic stressors. Figure 9B is the Mito Stress Test data output.

ATP Production Oxygen Consumption Rate (OCR) (Figure 9C) is the rate of oxygen consumption by the electron transport chain to create the proton gradient used by ATP synthase in the production of ATP. ATP Production OCR gives insight into how a cell produces energy. High ATP production results from increased ATP demand, while decreased ATP Production could be due to decreased substrate availability (NADH, $FADH_2$), electron transport chain damage, or decreased ATP demand. Oligomycin A and Antimycin A/Rotenone were used to determine ATP Production. ATP Production oxygen consumption rates (mean ± SEM) in fmol O_2/min/cell are: 1.7 ± 0.3 for NHSC, 14 ± 1 for STS26T, 3.3 ± 0.6 for ST88-14, 3.7 ± 0.5 for 90-8, and 3.6 ± 0.6 for S462 (Figure 9C). STS26T were significantly higher than all other cell types. NHSC, ST88-14, 90-8, and S462 lines do not have significantly different ATP production. NF1-deficient MPNST lines experience lower mitochondrial ATP Production OCR compared to NF1-wildtype.

Maximal Respiration OCR (Figure 9D) describes the fastest mitochondrial respiratory rate possible and indicates the cellular potential for mitochondrial respiration. An increased Maximal Respiration may result from increased mitochondrial mass, increased substrate availability, and efficient movement of electrons through the ETC while a decreased Maximal Respiration may result from

decreased mitochondrial mass, decreased substrate availability, and impaired electron movement through the ETC (Hill et al., 2012). Maximal Respiration is determined using FCCP and Antimycin A/Rotenone. The Maximal Respiration OCR (mean ± SEM) in fmol O_2/min/cell are: 3.9 ± 0.4 for NHSC, 41 ± 2 for STS26T, 13 ± 1 for ST88-14, 6.9 ± 0.6 for 90-8, and 10 ± 1 for S462 (Figure 9D). The NF1-wildype, STS26T, has significantly higher Maximal Respiration OCR than all other cells types. NHSC are significantly lower than STS26T, ST88-14, and S462. The NF1-deficient MPNST lines are not significantly different from each other but are significantly less than STS26T.

Spare Respiratory Capacity OCR (Figure 9E) reports how efficacious cells could be at mitigating energy crises via mitochondrial respiration. Cell lines with high Spare Respiratory Capacities may easily increase respiration to compensate for increased energy demand. Spare Respiratory Capacity OCR were identified using FCCP and Antimycin A/Rotenone. The Spare Respiratory Capacity OCR (mean ± SEM) in fmol O_2/min/cell are: 1.9 ± 0.4 for NHSC, 25 ± 2 for STS26T, 8 ± 1 for ST88-14, 3.1 ± 0.8 for 90-8, and 6 ± 1 for S462 (Figure 9E). All MPNST Spare Respiratory Capacities are higher than NHSC with only STS26T and ST88-14 being significantly so. STS26T was significantly higher than NF1-deficient MPNST and NHSC. NF1-deficient MPNST were not significantly different from each other.

FIGURE 9

NF1-deficient MPNST have lower mitochondrial respiration than NF1-wildtype

(A) Representative depiction of a Mitochondria Stress Test (B) Mitochondria Stress Test output for NHSC and MPNST lines (C) ATP Production oxygen consumption rates for NHSC and MPNST lines. (D) Maximal oxygen consumption rates for NHSC and MPNST lines (E) Spare Respiratory Capacities. Results are mean ± SEM. n = 5-10. P values determined by one-way ANOVA with Tukey post hoc. Oligomycin (A) = inhibits ATP synthase, FCCP = dissipates the electrochemical proton gradient, Rotenone = inhibits Complex I, Antimycin A = inhibits Complex III.

FIGURE 9

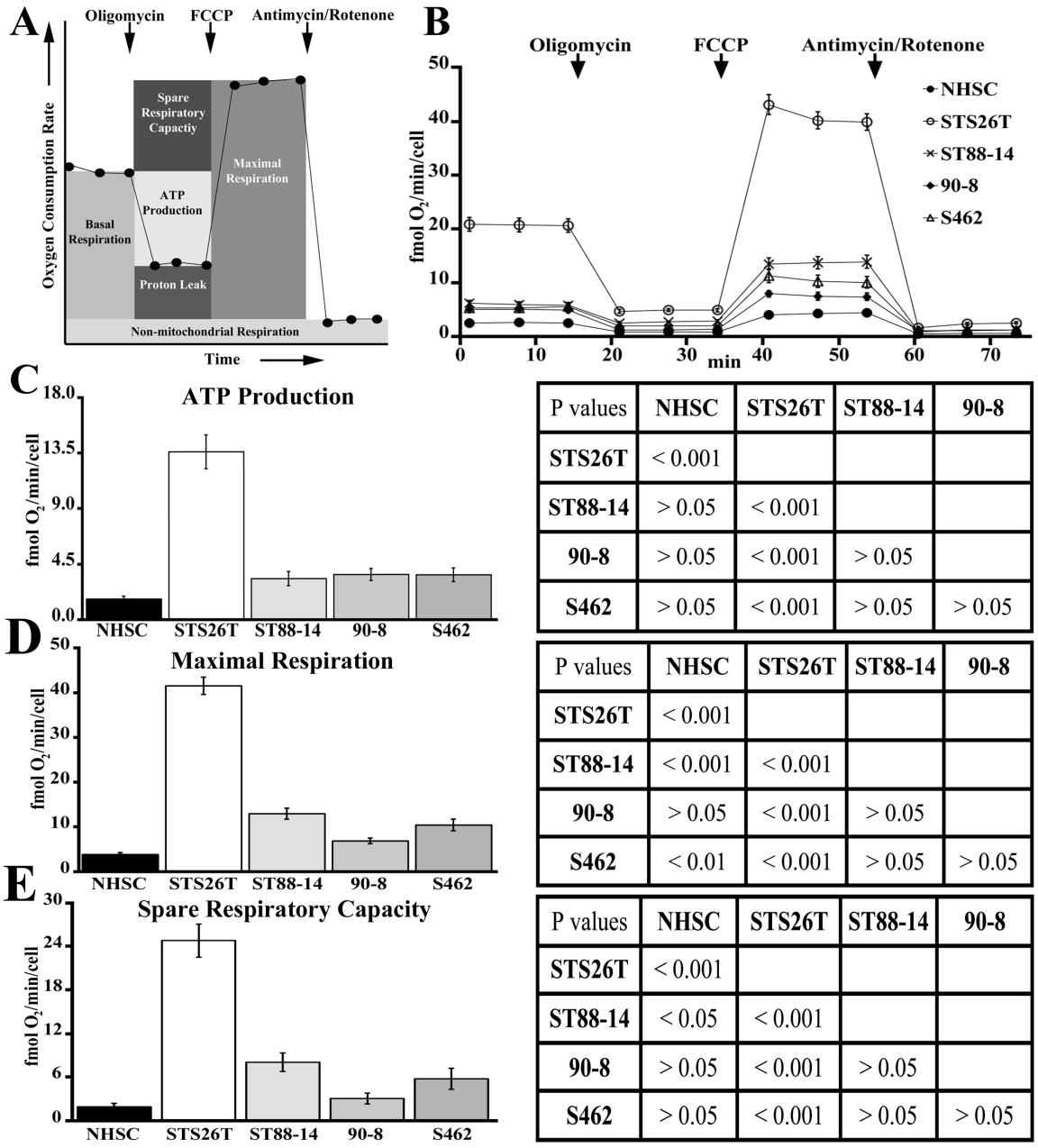

P values	NHSC	STS26T	ST88-14	90-8
STS26T	< 0.001			
ST88-14	> 0.05	< 0.001		
90-8	> 0.05	< 0.001	> 0.05	
S462	> 0.05	< 0.001	> 0.05	> 0.05

P values	NHSC	STS26T	ST88-14	90-8
STS26T	< 0.001			
ST88-14	< 0.001	< 0.001		
90-8	> 0.05	< 0.001	> 0.05	
S462	< 0.01	< 0.001	> 0.05	> 0.05

P values	NHSC	STS26T	ST88-14	90-8
STS26T	< 0.001			
ST88-14	< 0.05	< 0.001		
90-8	> 0.05	< 0.001	> 0.05	
S462	> 0.05	< 0.001	> 0.05	> 0.05

NF1-DEFICIENT MPNST LINES ARE LESS METABOLIC THAN NF1-WILDTYPE

Basal Respiration (Figure 9B) is the rate of oxygen consumed at rest. Basal Respiration, in a tumor model, has important implications in explaining the energy production capabilities of genetically dissimilar cells concerning temporal and spatial differences within a tumor microenvironment. Increased respiration may be the result of increased ATP turnover or proton leak. While decreased respiration is caused by decreased ATP demand, proton leak, substrate supply or inhibition of Complexes I-V. Antimycin A/Rotenone were used to test Basal Respiration. The Basal Respiration OCR (mean ± SEM) in fmol O_2/min/cell are: 2.0 ± 0.3 for NHSC, 17 ± 1 for STS26T, 4.9 ± 0.5 for ST88-14, 3.8 ± 0.5 for 90-8, 4.7 ± 0.5 for S462 (Figure 9B). STS26T was significantly higher than NHSC and NF1-deficient MPNST lines. NF1-deficient MPNST Basal Respirations were not significantly different from NHSC.

A metabolic profile aggregate, termed PhenoGram (Figure 10B) illustrates the metabolic differences between NF1-wildtype and NF1-deficient MPNST lines. All of the MPNST lines are shifted to the right of NHSC indicating a higher basal glycolysis than the NHSC. The Glycolysis ECAR (mean ± SEM) in μpH/min/cell are: 0.14 ± 0.02 for NHSC, 0.77 ± 0.07 for STS26T, 0.24 ± 0.01 for ST88-14, 0.30 ± 0.03 for 90-8, 0.62 ± 0.02 for S462 (Figure 8C). The NF1-deficient MPNST cell lines have lower Basal Respiration than STS26T and are the same as NHSC (Figure 9B). The effect of NF1 loss on MPNST cell line metabolism is apparent.

FIGURE 10

NF1-deficient MPNST lines are less metabolic than NF1-wildtype

Glycolytic and Basal Respiratory Rates plotted on the x- and y- axis, respectively. (A) Representative PhenoGram depicting metabolic shift to a more glycolytic state. (B) NHSC and MPNST PhenoGram. Note that NF1-deficient MPNST lines (surrounded in the box) are more metabolic than NHSC but less metabolic than NF1-wildtype.

FIGURE 10

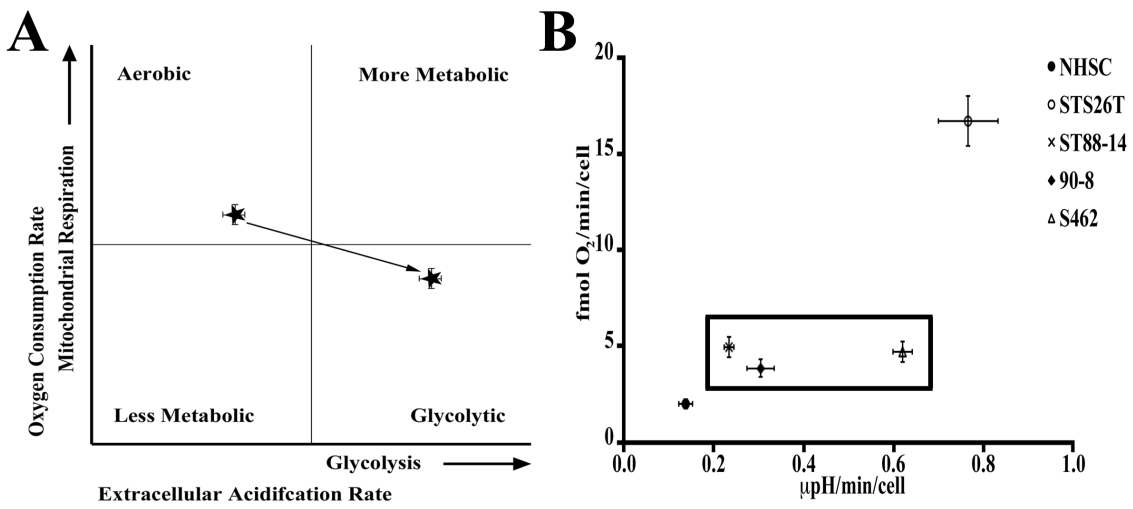
A
Aerobic
More Metabolic
Less Metabolic
Glycolytic
Oxygen Consumption Rate
Mitochondrial Respiration
Glycolysis
Extracellular Acidifcation Rate
B
fmol O2/min/cell
μpH/min/cell
0
5
10
15
20
0.0
0.2
0.4
0.6
0.8
1.0
NHSC
STS26T
ST88-14
90-8
S462

DIFFERENTIAL MPNST CELL LINE ELECTRON TRANSPORT CHAIN PROTEIN EXPRESSION

Western Blotting was used to determine whether the differences in mitochondria respiration were due to protein expression (Figure 11B). STS26T was the only cell line to have comparable or increased expression of all electron transport chain complexes compared to NHSC. The NF1-deficient MPNST cell lines have decreased expression of at least one respiratory complex compared to NHSC. Complex I subunit NDUFB8 was 0.3 fold lower than NHSC. Cytochrome C was 0.2 fold lower than NHSC in ST88-14 and 0.1 fold lower in S462. Complex IV subunit IV was 0.4 fold lower in 90-8 compared to NHSC. Complex V subunit alpha was 0.1 fold lower in STS26T, 0.7 fold lower in ST88-14, 0.2 fold lower in 90-8, and 0.4 fold lower in S462 compared to NHSC. All NF1-deficient MPNST cell lines had lower mitochondrial protein expression than NF1-wildtype MPNST. Protein loading was equal as illustrated by β-actin. Quantitation was relative to NHSC. Western blots shown are representative of two independent experiments.

FIGURE 11

Differential expression of Mitochondrial Respiratory Proteins in MPNST

(A) Illustration of the ETC with election and proton flow (B) Western Blot analysis of ETC Complex protein expression. Quantitation relative to NHSC. Western blots shown are representative of at least two independent experiments. ETC = electron transport chain, Complex I = NADH dehydrogenase, Complex II = succinate dehydrogenase, Q = coenzyme Q, Complex III = coenzyme Q-cytochrome C reductase, Cyto C = cytochrome C, Complex IV = cytochrome C oxidase, Complex V = ATP synthase

FIGURE 11

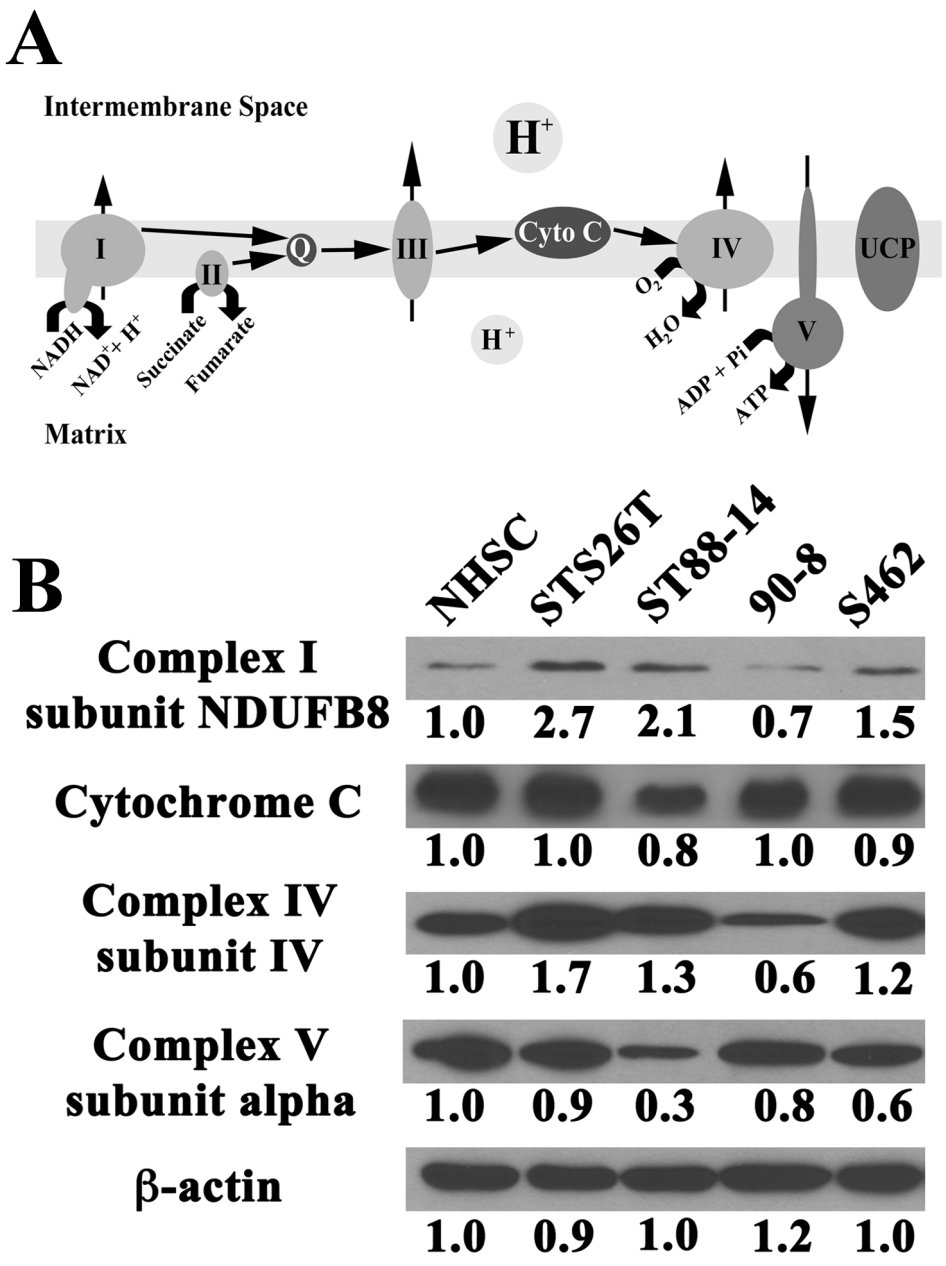
A
Intermembrane Space
H+
I
II
Q
III
Cyto C
IV
V
UCP
NADH
NAD+ + H+
Succinate
Fumarate
O2
H2O
H+
ADP + Pi
ATP
Matrix
B
NHSC
STS26T
ST88-14
90-8
S462
Complex I subunit NDUFB8
1.0 2.7 2.1 0.7 1.5
Cytochrome C
1.0 1.0 0.8 1.0 0.9
Complex IV subunit IV
1.0 1.7 1.3 0.6 1.2
Complex V subunit alpha
1.0 0.9 0.3 0.8 0.6
β-actin
1.0 0.9 1.0 1.2 1.0

NF1-DEFICIENT MPNST HAVE DECREASED UNCOUPLING

Proton Leak OCR (Figure 12C) is the rate of oxygen consumed by the electron transport chain to produce the proton gradient lost via proton leak. Proton leak via mitochondrial uncoupling proteins (UCP) has a regulatory role in ROS production and oxidative stress by acting as a throttle for the electron transport chain and ATP synthase (Jastroch et al., 2010). Proton Leak may be increased in response to: damaged electron transport chain (ETC) proteins, damaged inner-membrane, electron slip, and increased uncoupling protein activity (Hill et al., 2012). Decreased UCP activity and a robust ETC and inner-membrane results in a decreased Proton Leak. The Proton Leak OCR (mean ± SEM) in fmol O_2/min/cell are: 0.30 ± 0.05 for NHSC, 3.1 ± 0.4 for STS26T, 1.6 ± 0.2 for ST88-14, 0.2 ± 0.2 for 90-8, and 1.0 ± 0.2 for S462. STS26T was significantly higher than all other cell lines. ST88-14 was significantly different from NHSC, STS26T, and 90-8. S462 was significantly higher than NHSC and 90-8.

Western Blotting was used to determine whether the differences in proton leak were due to protein expression (Figure 12B). STS26T had the highest expression levels of UCP2 followed by ST88-14, then NHSC and 90-8. S462 had the lowest expression of UCP2. UCP2 expression closely mirrored proton leak activity measured by Extracellular Flux analysis (Figure 12C). Protein loading was equal as illustrated by β-actin. Quantitation was relative to NHSC. Western blots shown are representative of two independent experiments.

FIGURE 12

NF1-deficient MPNST lines have decreased Proton Leak

(A) ETC illustration with UCP. (B) Western Blot analysis of UCP2 protein expression. Quantitation relative to NHSC. Western blots shown are representative of at least two independent experiments. (C) NHSC and MPNST Proton Leak oxygen consumption rates. Results are mean ± SEM. n=5-10. P values determined by one-way ANOVA with Tukey post hoc. UCP = mitochondrial uncoupling protein

FIGURE 12

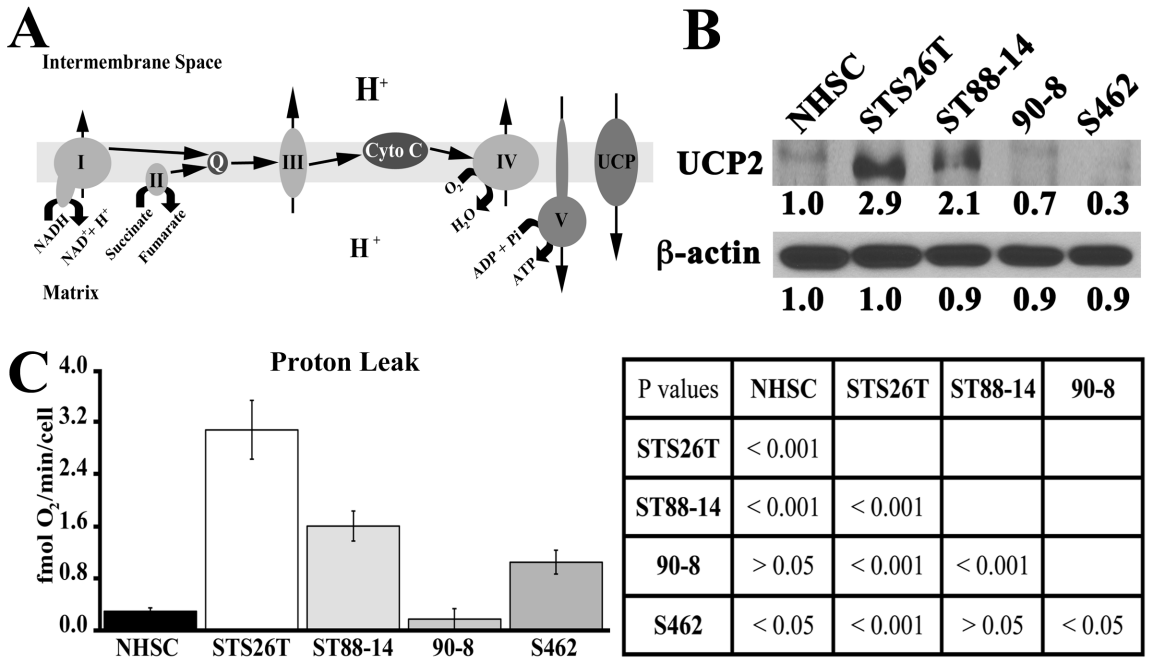

P values	NHSC	STS26T	ST88-14	90-8
STS26T	< 0.001			
ST88-14	< 0.001	< 0.001		
90-8	> 0.05	< 0.001	< 0.001	
S462	< 0.05	< 0.001	> 0.05	< 0.05

MPNST CELL LINE ROS ORIGINATE FROM MITOCHONDRIA

Extra-mitochondrial sources of ROS like nitric oxide synthase, xanthine oxidase, and lipoxygenase consume oxygen to produce reactive oxygen species (Hill et al., 2012). ROS are capable of damaging DNA and proteins, and create havoc by disrupting intercellular signaling. Dichlorofluorescin (DCF) fluorescence measured ROS levels to further characterize the apparent respiratory dysfunction (Figure 13B). The fold change in ROS from NHSC (mean ± SEM) are: 1.0 ± 0.1 for NHSC, 4.8 ± 0.3 for STS26T, 2.7 ± 0.1 for ST88-14, 3.2 ± 0.2 for 90-8, and 1.7 ± 0.1 for S462. STS26T was significantly higher than all other cells types. ST88-14, 90-8, and S462 were all significantly different from each other and higher than NHSC.

Non-mitochondrial Respiration OCR (Figure 13C) is the rate of oxygen consumed to fuel other oxygen utilizing processes. Increased Non-mitochondrial OCR may indicate increased ROS production through extra-mitochondrial enzymes (like nitric oxide synthases) while lower Non-mitochondria-derived OCR indicates decreased non-mitochondrial ROS production. Antimycin A/Rotenone were used to determine Non-mitochondria OCR. The Non-mitochondria-derived OCR (mean ± SEM) in fmol O_2/min/cell are: 0.56 ± 0.02 for NHSC, 1.7 ± 0.2 for STS26T, 1.0 ± 0.1 for ST88-14, 1.1 ± 0.1 for 90-8, and 0.9 ± 0.1 for S462. STS26T is significantly higher than all other cell lines apart from 90-8. The NF1-deficient MPNST cell lines were not significantly different from each other or NHSC. Nitric oxide synthase (NOS) is a possible source of non-mitochondrial oxygen consumption (Figure 13D). eNOS and nNOS protein expression was evaluated by Western blot analysis. eNOS expression

was found to be lower in MPNST cell lines than NHSC and nNOS expression was also found to be lower in MPNST cell lines than NHSC with the exception of S462.

FIGURE 13

MPNST cell line ROS originate from mitochondria

(A) Schematic detailing mitochondrial production of ROS. (B) ROS levels as fold change from NHSC. n=8. (C) Non-mitochondrial oxygen consumption rates. n=5-10. Results are mean ± SEM. P values determined by one-way ANOVA with Tukey post hoc (D) Western blot analysis of eNOS and nNOS expression. Quantitation relative to NHSC. Even protein loading determined by β-actin expression. Western blots shown are representative of at least two independent experiments. eNOS = endothelial Nitric Oxide Synthase, nNOS = neuronal Nitric Oxide Synthase.

FIGURE 13

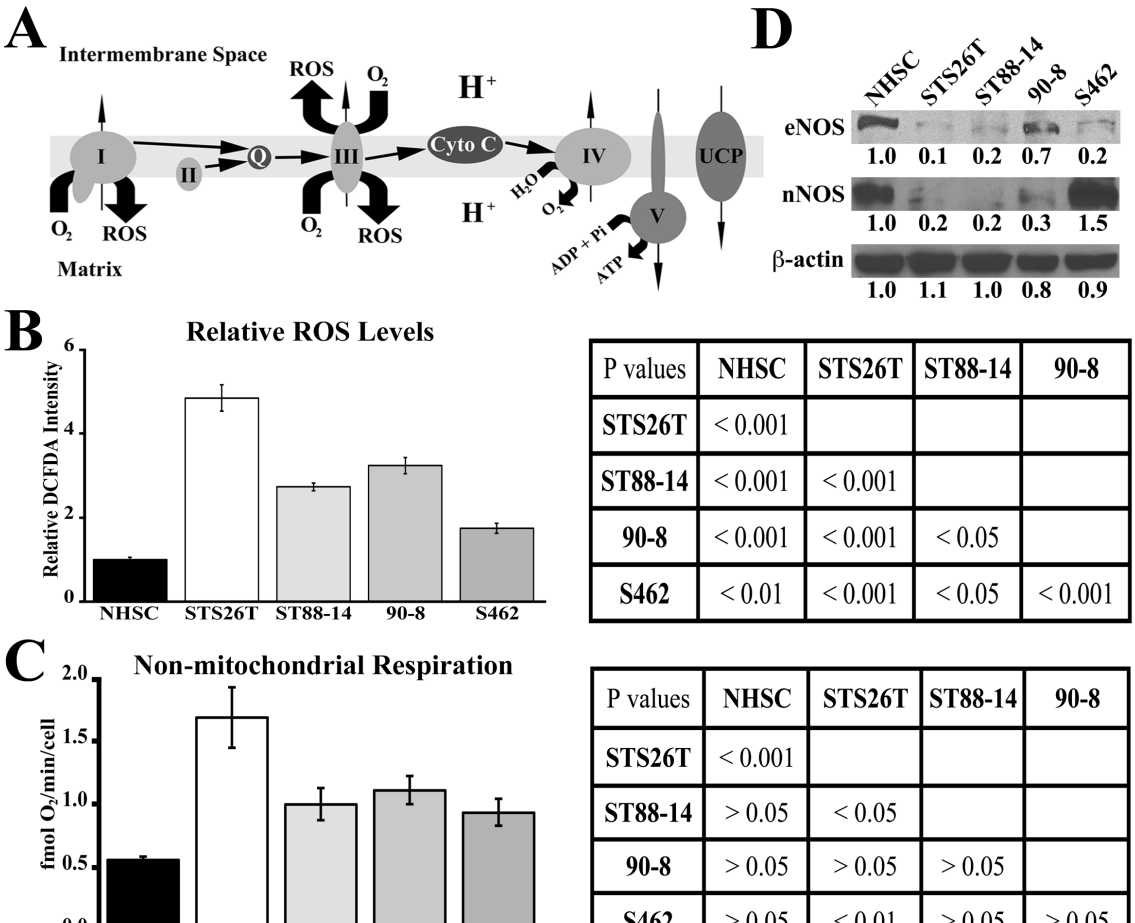

P values	NHSC	STS26T	ST88-14	90-8
STS26T	< 0.001			
ST88-14	< 0.001	< 0.001		
90-8	< 0.001	< 0.001	< 0.05	
S462	< 0.01	< 0.001	< 0.05	< 0.001

P values	NHSC	STS26T	ST88-14	90-8
STS26T	< 0.001			
ST88-14	> 0.05	< 0.05		
90-8	> 0.05	> 0.05	> 0.05	
S462	> 0.05	< 0.01	> 0.05	> 0.05

DISCUSSION

Similar to other tumors and tumor cell lines, the MPNST cell lines examined in this study exhibited the increased glycolytic rates noted in the Warburg effect when compared to a non-tumorigenic NHSC line. One explanation for this change may be because glycolysis produces ATP faster than oxidative phosphorylation. Tumor cells may shift to a more glycolytic state in order to maintain the energy requirements necessary for sustained elevation of cellular proliferation – especially in a nutrient-deprived, hypoxic environment. Testing whether a hypoxic environment would cause this switch in our cells was not performed, but is possible to do in our system using a hypoxia chamber and varying nutrient concentrations in cellular media. Our findings that all tumor lines had faster glycolysis than normal Schwann cells are consistent with the notion that the tumor lines have higher growth rate and energy demands.

Hyperactivation of the Ras pathway has been found in many tumor types; therefore, it is interesting that patients with Neurofibromatosis Type I have a higher incidence of MPNST. Patients with NF1 have a genetic mutation or loss of function of the *NF1* gene, encoding the neurofibromin protein. Since NF1 is a Ras-GTPase, it acts to turn the Ras pathway off. NF1-deficient cells have increased Ras-MAPK signaling. Previous reports have linked Ras hyperactivation to an increase in glycolysis in embryonic fibroblasts (de Groof et al., 2009). Our findings that Nf1-deficient MPNST cell lines have lower glycolytic rates compared to an NF1-wildtype MPNST cell line diverges with previous studies involving the Ras pathway in non-tumorigenic cells suggesting that the loss of NF1/hyperactivation of Ras may decrease glycolytic rates

in MPNST. All MPNST cell lines did have higher glycolytic rates than normal Schwann cells.

The role of Ras on mitochondrial respiration has been controversial, but the consensus seems to be that Ras hyperactivation results in decreased mitochondrial respiration (Telang et al., 2007, de Groof et al., 2009, Yang and Wang et al., 2010, and Hu, Lu and Chen et al., 2012). Conclusions made from the Hu, Lu, and Chen et al., 2012 article should be made cautiously as doxycycline was used to induce Ras hyperactivation and the tetracycline family of antibiotics, of which doxycycline is a member, are known to directly decrease proliferation and shift metabolism to a more glycolytic phenotype while decreasing mitochondrial respiration (Ahler and Sullivan et al., 2012). Wang and Song recently identified that K-Ras hyperactivation caused mitochondrial dysfunction by decreasing NADH dehydrogenase 1 alpha subcomplex assembly factor 1 (NDUFAF1) expression (Wang and Song et al., 2015). NDUFAF1 is a protein involved in the assembly of Complex 1. Other studies have demonstrated a decrease in Complex 1 activity upon Ras transformation that is connected with the mitochondrial respiratory depression (Baracca et al., 2010). Further research is needed to determine the extent of Ras impact on mitochondria.

Several studies have evaluated the effect of Ras hyperactivation on mitochondrial respiration but not as many studies have been done to determine whether Ras directly effects glycolysis. One of the few studies found that Ras-induced changes in glycolysis are regulated by 6-Phosphofructo-2-Kinase/Fructose-2,6-Bisphosphatase 3 (PFKFB3) activity in murine lung fibroblasts (Telang et al., 2009). PFKB3 increased fructose 2,6-biphosphate (F-2,6-BP) levels upon Ras

hyperactivation. F-2,6-BP increases glycolysis through allosteric activation phosphofructokinase-1 (PFK-1) by increasing PFK-1 affinity for fructose 6-phosphate and decreasing its affinity for the allosteric inhibitors, ATP and citrate. PFK-1 is a crucial regulatory step in glycolysis. Given these findings, it is reasonable to hypothesize that F 2,6-BP is increased in the MPNST cell lines derived from NF1 patients and assists in generation of the increased glycolytic state observed. Future experiments may examine this point.

The finding that NF1-deficient MPNST cell lines have significantly lower glycolysis than that found in the NF1-expressing MPNST line was surprising. NF1-deficient MPNST cell lines were also significantly less metabolic with lower oxygen consumption rates, maximal respiration, and spare respiratory capacity than NF1-wildtype, indicating the capability of NF1-deficient tumor cell lines to produce energy via oxidative phosphorylation is considerably lower than NF1-wildtype malignant cells.

When we compared the various NF1-deficient MPNST cell lines to one another, they all responded in a similar manner to metabolic stress, with more variability noted in glycolytic rates than overall metabolism. Increases in both glycolytic and mitochondrial respiration indicate more energetic cells when compared to wildtype, non-tumorigenic NHSC. The variability between the NF1-deficient MPNST lines examined in this study was substantial, with more striking differences shown between the NF1-deficient ST88-14 line and the NF1-wildtype STS26T cell line which are historically the most commonly compared lines for NF1 loss changes.

All of the MPNST cell lines (regardless of NF1 status) have multiple genetic mutations. The genetic mutation(s) within the lines examined in this study has not been identified, as full genetic sequencing has not been preformed. Therefore, investigators have historically assumed that any differences observed between NF1-deficient MPNST lines could be attributable to variations in cell line history and/or genetics. Although we did see individual expression differences in specific subunits of the Complexes in each of the cell lines, this could be one reason that we did not find any specific or distinct pattern(s) in respiratory protein expression that we think could fully explain the metabolic activity measurements obtained through Extracellular Flux analysis. Furthermore, these mitochondrial complexes are composed of a multitude of subunits that could not be segregated out using the antibodies that are currently available. Mass spectrometric analysis of mitochondrial respiratory complexes has been used previously and may provide a more complete accounting of the subunits expressed and in what ratios (Schilling and M. M. et al., 2005).

Previous research using the same cell lines used in this study and other MPNST lines (both NF1-wildtype and NF1-deficient) claim that NF1 status does not have an impact on proliferation rate (Miller et al., 2006). This article used an MTT assay as a measure of cellular proliferation, which is a common practice in many labs. However, the MTT assay is not always a good indicator of proliferation as it actually measures NAD(P)H-dependent oxidoreductase (Complex I) activity in the reduction of MTT to the insoluble and detectable tetrazolium dye. There is a correlation between high MTT results and proliferating cells because as cells divide

their energy consumption goes up. However, differences in metabolism can also alter MTT without a change in proliferation rates. For example, if cells are less efficient at utilizing energy, then a higher MTT will result – especially if they obtain more of their energy from glycolysis and not mitochondrial respiration. For this reason, I propose that both MTT and proliferation counts be performed to more accurately characterize how NF1 status may effect proliferation rates and/or metabolism changes in these cell lines.

Proton leak through uncoupling proteins (UCP) acts as a throttle for mitochondrial respiration. We found that NF1-deficient MPNST have lower rates of proton leak than the NF1-wildtype MPNST cell line and proton leak activity closely mirrors UCP2 expression with the exception of S462. The observation that UCP2 expression does not reflect proton leak in S462 could be due to: the S462 line may express a different uncoupling protein or UCP2 in S462 may undergo different post-translational modifications that alter the size of the protein and change its location on the western blot membrane. Proton leak can be changed by multiple factors beyond UCP protein expression – such as damage to the membrane or electron transport chain protein(s). Therefore, while the proton leak we noted in the extracellular flux data correspond nicely with UCP expression data, it is probable that other factors also play a role. Superoxide (a reactive oxygen species) production is responsive to changes in the proton-motive force via uncoupling proteins (Jastroch et al., 2010). The decreased activity and expression of UCP2 in NF1-deficient MPNST compared to NF1-wildtype MPNST indicates decreased electron transport chain control and highlights the possibility of increased reactive

oxygen species (ROS) production in NF1-deficient MPNST cells compared to wildtype MPNST. Moderate uncoupling helps prevent the build up of substrate at the respiratory proteins and may decrease premature electron removal from the transport chain and creation of reactive oxygen species.

Mitochondria are the major producer of cellular reactive oxygen species. ROS are an unavoidable byproduct of mitochondrial respiration and increased ROS are routinely observed in cancer cells. ROS are implicated in tumor progression and persistence of the malignant state through activation of transcription factors like HIF-1α and FOS-JUN that will modify protein expression and promote cell proliferation (Wallace 2012). ROS can further exacerbate tumorgenicity by activating ERK1/2, a member of the MAPK pathway downstream of Ras (Weinberg et al., 2010). ROS are involved in NF1 behavioral deficits (Mayes et al., 2013). ROS levels were examined using CM-H_2DCFDA—a general indicator of oxidative stress (Kuznetsov et al., 2011). DCF, the fluorescent product, responds to superoxide, nitric oxide, and peroxynitrite, among several other reactive oxygen species. MPNST have higher ROS relative to NHSC with NF1-deficient having significantly lower levels of ROS than NF1-wildtype MPNST.

The increased ROS observed in the NF1-deficient MPNST cells compared to NHSC originate from the mitochondria because the NF1-deficient MPNST Non-mitochondrial oxygen consumption rates are not significantly different from NHSC, meaning that the other processes within the cells that utilize oxygen are not consuming oxygen at different rates. The NF1-wildtype MPNST cell line has significantly higher Non-mitochondrial respiration from two of the NF1-deficient

lines and NHSC, indicating that the NF1-wildtype MPNST cells have an increased oxygen utilization for processes other than respiration. NF1-wildtype is not different from one of the NF1-deficient cell lines.

Nitric oxide synthase had previously been shown culpable in the generation of NF1-cognitive and behavioral phenotypes. NOS produces nitric oxide (NO) which is a ROS. NOS protein expression levels were examined using Western blot analysis; however, no specific trends were noted between the lines. Most of the lines did not express eNOS and nNOS isoforms while NHSC did. The increased ROS observed in NF1-deficient could be a result of electron transport chain damage due to mutations or other mitochondrial dysfunction. An alternate possibility is that there is a reduction in ROS scavenging by superoxide dismutase 2 (SOD2).

The final point is perhaps the most tenuous. The NF1-wildtype MPNST cell line (ST26T) had significantly higher mitochondrial respiration than NHSC, more than 8 times higher while producing 5 times as much ROS. While in contrast the NF1-deficient MPNST lines had about 2 times faster mitochondrial respiration (not significantly different) and produce about 3 times as much ROS. Together these data suggest that the MPNST lines derived from NF1 patients are producing more ROS for their respiratory rate than the wildtype MPNST line, perhaps indicating a higher degree of mitochondrial dysfunction in the Ras transformed tumor cells than sporadic tumor cells.

In summary, we found significant differences in glycolysis and mitochondrial respiratory rates and respiratory protein expression between NF1-wildtype and NF1-deficient MPNST cells. These differences alter the way the cells produce energy

and mitigate energy crises. The mitochondrial respiratory dysfunction influences proliferation and ROS generation. The observations described in this thesis should increase the caution of researchers using these MPNST cell lines, as they highlight the fact that each MPNST have fundamentally different metabolic profiles, which may influence their response(s) in vitro and in vivo.

FUTURE EXPERIMENTS

To strengthen the findings that NF1-deficient MPNST cell lines have decreased mitochondrial respiration and to suggest an explanation as to why the cell lines behave the ways they do, several more experiments should be done.

Probing the MPNST cell lines for the expression of S100 protein using immunocytochemistry will indicate how similar MPNST cells are to NHSC. S100 is a family of proteins expressed in cells derived from the neural crest and is used as a marker for Schwann cells. If MPNST cell lines no longer express S100 then the cell lines have degenerated far from what their cell of origin is thought to be and caution should be used when comparing NHSC and MPNST cell lines as NHSC may no longer be a good normal control cell for MPNST cell lines. Previous research claims that S100 is not expressed in MPNST cell lines (Miller et al., 2006).

Another experiment that should be done is a cell proliferation assay. Proliferation data has been previously published using a MTT assay. In light of the findings within this document the MTT assay is not a good measure of cellular proliferation because the MTT assay is thought to actually measure NAD(P)H turnover at NAD(P)H oxidoreductases, like Complex I. Within metabolically remodeled cells, a technique based on the measurement of one energy production pathway and interpreted, as proliferation is erroneous because NF1-wildtype and NF1-defiecent MPNST cell lines have drastically different mitochondrial respiration rates. Therefore, a technique measuring substrate turnover may not accurately represent proliferative rates because two major pathways of energy production

exist. A series of direct cell counts over several days should provide the most accurate information and allow for correlation of metabolic rates to proliferation.

The last experiment would be to determine the mitochondrial volume for the cell lines via immunocytochemistry. Mitochondrial volume can serve as a surrogate for mitochondria amount. The mitochondrial volume can be determined using TOM20 to reveal mitochondria and Na+/K+ ATPase to show the total cell volume. Mitochondrial volume would be normalize to cellular volume. If the mitochondrial volume was the same for all lines then the differences in mitochondrial respiration would be a result of activity regulation and some protein expression. While if significant differences were found between the sporadic MPNST and NF1-deficient MPNST lines then it would be indicative of a greater systemic problem such as increased mitophagy or mitochondrial biogenesis.

Determing whether MPNST cell lines derived from NF1 patients have greater mitophagy than wildtype MPNST would greatly influence the conclusions of this study. The findings of the experiment may provide evidence for the claim that the decreased mitochondrial respiration observed in NF1-deficient MPNST cell lines may be caused, in part, by increased mitophagy. Perhaps a good method to determine amount of mitophagy in a given cell would be to measure the colocalization of TOM20 and LC3B proteins using immunofluorescence microscopy. TOM20 is found on mitochondrial membranes and is used to translocate mitochondria proteins to mitochondrial membranes. LC3B is involved in formation of autophagosomes and is used as a marker for autophagic membranes. Autophagosomes traffic cellular components to lysosomes for degradation. The two

proteins would be probed with different fluorescent probes and then imaging software would calculate the amount of overlap the two different wavelengths have within a single pixel and produce a colocalization value. A higher value of colocalization indicates that there is a greater amount of overlap between mitochondria and autophagosome membranes meaning a higher amount of mitophagy. If the levels of mitophagy in NF1-deficient MPNST cell lines are higher than wildtype MPNST then mitophagy may be contributing to the lower mitochondrial respiration observed. If the levels of mitophagy are not different between the two types of MPNST then the decreased mitochondrial respiration observed is probably caused by some other mechanism (for example; directly changing enzymatic activity).

REFERENCES

Ahler E., Sullivan W.J., Cass A., Braas D., York A.G., Bensinger S.J., Graeber T.G., and Christofk H.R., 2013. Doxycycline Alters Metabolism and Proliferation of Human Cell Lines. *PLoS ONE* **8(5)**:e64561

Amigoni L., Martegani E., and Colombo S., 2013. Lack of HXK2 Induces Localization of Active Ras in Mitochondria and Triggers Apoptosis in the Yeast Saccharomyces cerevisiae. *Oxidative Medicine and Cellular Longevity*; **2013**: 678473

Anghileri, M., Miceli, R., Fiore, M., Mariani, L., Ferrari, A., Mussi, C., Lozza, L., Collini, P., Olmi, P., Casali, P. G., Pilotti, S., and Gronchi, A., 2006. Malignant peripheral nerve sheath tumors: prognostic factors and survival in a series of patients treated at a single institution. *Cancer*; **107**:1065-1074

Ballester R., Marchuk D., Boguski M., Saulino A., Letcher R., Wigler M., Collins F., 1990. The NF1 locus encodes a protein functionally related to mammalian GAP and yeast IRA proteins. *Cell*; **63(4)**:851-859

Baracca A., Chiaradonna F., Sgarbi G., Solaini G., Alberghina L., Lenaz G., 2010. Mitochondrial Complex I decrease is responsible for bioenergetic dysfunction in K-ras transformed cells. *Biochimica et Biophysica Acta*; **1797(2)**:314-23

Bensaad K., Tsuruta A., Selak M.A., Vidal M.N.C., Nakano K., Bartrons R., Gottlieb E., Vousden K.H., 2006. TIGAR, a p53-Inducible Regulator of Glycolysis and Apoptosis. *Cell*; 1**26(1)**:107-120

Boland M.L., Chourasia A.H., Macleod K.F., 2013. Mitochondrial Dysfunction in Cancer. *Frontiers in Oncology*; **2013(3)**:292

Cawthon R.M., O'Connell P., Buchberg R.M., Viskochil D., Weiss R.B., Culver M., Stevens J., Jenkins N.A., Copeland N.G., and White R., 1990. Identification and characterization of transcripts from the neurofibromatosis 1 region: The sequence and genomic structure of EVI2 and mapping of other transcripts. *Genomics*; **7(4)**:555-565

Chen X., Qian Y., and Wu S., 2015. The Warburg effect: Evolving interpretations of an established concept. *Free Radical Biology and Medicine*; **79**:253-263

Clem B., Telang S., Clem A. Yalcin A., Meier J., Simmon A., Rasku M.A., Arumugam S., Dean W.L. Eaton J., Lane A., Trent J.O., Chesney J., 2008. Small-molecule inhibition of 6-phosphofructo-2-kinase activity suppresses glycolytic flux and tumor growth. *Mol Cancer Ther*; **7(1)**:110-20

De Groof A.J., te Lindert M.M., van Dommelen M.M.T., Wu M., Willemse M., Smift A., Winer M., Oerlemans F., Pluk H., Fransen J.A.M., and Wiering B., 2009. Increased OXPHOS activity precedes rise in glycolytic rate in H-RasV12/E1A transformed fibroblasts that develop a Warburg phenotype. *Molecular Cancer*; **8**:54

Doorn, P. F., Molenaar, W. M., Buter, J., and Hoekstra, H. J., 1995. Malignant peripheral nerve sheath tumors in patients with and without neurofibromatosis. *Eur J Surg Oncol*; **21**:78-82

Ducatman, B. S., Scheithauer, B. W., Piepgras, D. G., Reiman, H. M., and Ilstrup, D. M., 1986. Malignant peripheral nerve sheath tumors. A clinicopathologic study of 120 cases. *Cancer;* **57**:2006-2021

Evans D., Baser M., McGaughran J., Sharif S., Howard E., Moran A., 2002. Malignant peripheral nerve sheath tumours in neurofibromatosis 1. *Journal of Medical Genetics*; **39(5)**:311-314

Ferner, R. E., and Gutmann, D. H., 2002. International consensus statement on malignant peripheral nerve sheath tumors in neurofibromatosis. *Cancer Res;* 1**62**:1573-1577

Ferner R.E., Huson S.M., Thomas N., Moss C., Willshaw H., Evans D.G., Upadhyaya M., Towers R., Gleeson M., Steiger C., Kirby A., 2007. Guidelines for the diagnosis and management of individuals with neurofibromatosis 1. *Journal of Medical Genetics*; **44(2)**:81-88.

Frank M., Duvezin-Caubet S., Koob S., Occhipinti A., Jagasia R., Petcherski A., Ruonala M.O, Priault M., Salin B., Reichert A.S., 2012. Mitophagy is triggered by mild oxidative stress in a mitochondrial fission dependent manner. *Biochimica et Biophysica Acta (BBA) - Molecular Cell Research*; **1823(12)**:2297-2310

Friedman, J.M., 1999. Epidemiology of neurofibromatosis type 1. *Am. J. Med. Genet*; **89**:1–6

Grobmyer, S. R., Reith, J. D., Shahlaee, A., Bush, C. H., and Hochwald, S. N., 2008. Malignant Peripheral Nerve Sheath Tumor: molecular pathogenesis and current management considerations. *JSurg Oncol*; **97**:340-349

Guo J.Y., Chen H-Y., Mathew R., Fan J., Strohecker A.M., Karsli-Uzunbas G., Kamphorst J.J., Chen G., Lemons J.M., Karantza V., Coller H.A., Dipaola R.S., Gelinas C., Rabionowitz J.D., and White E., 2011. Activated Ras requires autophagy to maintain oxidative metabolism and tumorigenesis. *Genes & Development*; **25(5)**:460-470.

Hill B.G., Benavides G.A., Lancaster J.R., Ballinger S., Dell'Italia L., Zhang J., Darley-Usmar V.M., 2012. Integration of cellular bioenergetics with mitochondrial quality control and autophagy. *Biological Chemistry*; **393(12)**:1485-1512

Hu Y., Lu W., Chen G., Wang P., Chen Z., Zhou Y., Ogasawara M., Trachootham D., Feng L., Pelicano H., Chiao P.J., Keating M., Garcia-Manero G., and Huang P., 2012. K-rasG12V transformation leads to mitochondrial dysfunction and a metabolic switch from oxidative phosphorylation to glycolysis. *Cell Research*; **22(2)**:399-412

Hyman, S. L., Shores, A., and North, K. N., 2005. The nature and frequency of cognitive deficits in children with neurofibromatosis type 1. *Neurology* **65**:1037-1044

Jastroch M., Divakaruni A.S., Mookerjee S., Treberg J.R., Brand M.D., 2010. Mitochondrial proton and electron leaks. *Essays in Biochemistry*; **47**:53-67

Jett, K., and Friedman, J. M., 2010. Clinical and genetic aspects of neurofibromatosis 1. *Genet Med* **12**:1-11

Kolberg M., Høland M., Ågesen T.H., Brekke H.R., Liestøl K., Hall K.S., Mertens F., Picci P., Smeland S., and Lothe R.A., 2013. Survival meta-analyses for >1800 malignant peripheral nerve sheath tumor patients with and without neurofibromatosis type 1. *Neuro Oncol*; **15(2)**:135-147

Kole H.K., Resnick R.J., Van Doren M., Racker E., 1991. Regulation of 6-phosphofructo-1-kinase activity in ras-transformed rat-1 fibroblasts. *Arch Biochem Biophys*; **286(2)**:586-90.

Kondoh H., Lleonart M.E., Gil J., Wang J., Degan P., Peters G., Martinez D., Carnero A., and Beach D., 2005. Glycolytic Enzymes Can Modulate Cellular Life Span. *Cancer Res*; **65**:177-185

Korf, B.R.,1999. Plexiform neurofibromas. *Am. J. Med. Genet.*; **89**: 31–37

Krab, L. C., Goorden, S. M., and Elgersma, Y., 2008. Oncogenes on my mind: ERK and MTOR signaling in cognitive diseases. *Trends Genet;* **24**:498-510

Kuznetsov A.V., Kehrer I., Kozlov A.V., Haller M., Redl H., Hermann M., Grimm M., Troppmair J., 2011. Mitochondrial ROS production under cellular stress: comparison of different detection methods. *Analytical and Bioanalytical Chemistry*; **400(8)**: 2383-2390.

Ledbetter D.H., Rich D.C., O'Connell P., Leppert M., Carey J.C., 1989. Precise localization of NF1 to 17q11.2 by balanced translocation. *American Journal of Human Genetics*; **44(1)**:20-24.

Lee, M. J., and Stephenson, D. A., 2007. Recent developments in neurofibromatosis type 1. *Curr Opin Neurol*; **20**:135-141

Maddocks O.D., Vousden K.H., 2011. Metabolic regulation by p53. *Journal of Molecular Medicine (Berlin, Germany)*; **89(3)**:237-245.

Mailloux R.J., Harper M.E., 2011. Uncoupling proteins and the control of mitochondrial reactive oxygen species production. *Free Radical Biology and Medicine*; **51(6)**:1106-1115.

Marchuk D.A., Saulino A.M., Tavakkol R., Swaroop M., Wallace M.R., Andersen L.B., Mitchell A.L., Gutmann D.H., Boguski M., Collins F.S., 1991. cDNA cloning of the type 1 neurofibromatosis gene: Complete sequence of the NF1 gene product. *Genomics*, **11(4)**:931-940

Martin G.A., Viskoohil D., Bollag G., McCabe P.C., Crosier W.J., Haubruck H., Conroy L., Clark R., O'Connell P., Cawthon R.M., Innis M.A., McCormick F., 1990. The GAP-related domain of the neurofibromatosis type 1 gene product interacts with ras p21. *Cell*; **63(4)**:843-849

Mattingly R.R., Kraniak J.M., Dilworth J.T., Mathieu P., Bealmear B., Nowak J.E., Benjamins J.A., Tainsky M.A., and Reiners, Jr. J.J., 2006. The Mitogen-Activated Protein Kinase/Extracellular Signal-Regulated Kinase Kinase Inhibitor PD184352 (CI-1040) Selectively Induces Apoptosis in Malignant Schwannoma Cell Lines. *J Pharmacol Exp Ther*; **316**:456-465

Mayes D.A., Rizvi T.A., Titus-Mitchell H., Oberst R., Ciraolo G.M., Vorhees C.V., Robinson A.P., Miller S.D., Cancelas J.A., Stemmer-Rachamimov A.O., Ratner N., 2013. *Nf1* Loss and Ras Hyperactivation in Oligodendrocytes Induce NOS-Driven Defects in Myelin and Vasculature. *Cell Reports*; **4(6)**:1197-1212

McClatchey, A. I., 2007. Neurofibromatosis. *Annu Rev Pathol*; **2**:191-216

Miller S.J., Rangwala F., Williams J., Ackerman P., Kong S., Jegga A.G., Kaiser S., Aronow B.J., Frahm S., Kluwe L., Mautner V., Upadhyaya M., Muir D., Wallace M., Hagen J., Quelle D.E., Watson M.A., Perry A., Gutmann D.H., and Ratner N., 2006. Large-Scale Molecular Comparison of Human Schwann Cells to Malignant Peripheral Nerve Sheath Tumor Cell Lines and Tissues. *Cancer Res*; **66**:2584-2591

Mitchell P., 1961. Coupling of phosphorylation to electron and hydrogen transfer by a chemi-osmotic type of mechanism. *Nature*; **191**:144-8

Nakajima E.C., Van Houten B.,2013. Metabolic symbiosis in cancer: Refocusing the Warburg lens. *Mol. Carcinog.*; **52**:329–337

Parrinello, S., and Lloyd, A. C., 2009. Neurofibroma development in NF1--insights into tumour initiation. *Trends Cell Biol*; **19**:395-403

Patel A.V., Eaves D., Jessen W.J., Rizvi T.A., Ecsedy J.A., Qian M.G., Aronow B.J., Perentesis, J.P., Serra E., Cripe T.P., Miller S.J., and Ratner N., 2012. Ras-Driven Transcriptome Analysis Identifies Aurora Kinase A as a Potential Malignant Peripheral Nerve Sheath Tumor Therapeutic Target. *Clin Cancer Res*; **18**:5020-5030

Porter, D. E., Prasad, V., Foster, L., Dall, G. F., Birch, R., and Grimer, R. J., 2009. Survival in Malignant Peripheral Nerve Sheath Tumours: A Comparison between Sporadic and Neurofibromatosis Type 1-Associated Tumours. *Sarcoma*; **2009**:756395

Rasmussen S.A., Yang Q., Friedman J.M., 2001. Mortality in Neurofibromatosis 1: An Analysis Using U.S. Death Certificates. *American Journal of Human Genetics*; **68(5)**:1110-1118.

Riccardi, V. M., 2010. Neurofibromatosis type 1 is a disorder of dysplasia: the importance of distinguishing features, consequences, and complications. *Birth Defects Res A Clin Mol Teratol*; **88**:9-14

Rosser, T. L., and Packer, R. J., 2003. Neurocognitive dysfunction in children with neurofibromatosis type 1. *Curr Neurol Neurosci Rep;* **3**:129-136

Roudebush M., Slabe T., SundaramV., Hoppel C.L., Golubic M., Stacey D.W., 1997. Neurofibromin Colocalizes with Mitochondria in Cultured Cells. *Experimental Cell Research*; **236(1)**:161-172

Schilling B., M.M. S.B., Row R.H., Murray J., Cusack M.P., Capaldi R.A., Freed C.R., Prasad K.N., Andersen J.K., and Gibson B.W., 2005. Rapid Purification and Mass Spectrometric Characterization of Mitochondrial NADH Dehydrogenase (Complex I) from Rodent Brain and a Dopaminergic Neuronal Cell Line. *Mol Cell Proteomics*; **4**: 84-96.

Serra E., Rosenbaum T., Winner U., Aledo R., Ars E., Estivill X., Lenard H., and Lázaro C., 2000. Schwann cells harbor the somatic *NF1* mutation in neurofibromas: evidence of two different Schwann cell subpopulations. *Hum. Mol. Genet.*; **9(20)**:3055-3064

Shilyansky, C., Lee, Y. S., and Silva, A. J., 2010. Molecular and cellular mechanisms of learning disabilities: a focus on NF1. *Annu Rev Neurosci;* **33**:221-243

Smith P.K., Krohn R.I., Hermanson G.T., Mallia A.K., Gartner F.H., Provenzano M.D., Fujimoto E.K., Goeke N.M., Olson B.J., Klenk D.C., 1985. Measurement of protein using bicinchoninic acid.*Analytical Biochemistry*; **150(1)**: 76-85

Staser, K., Yang, F. C., and Clapp, D. W., 2010. Mast cells and the neurofibroma microenvironment**.** *Blood*; **116**:157-164

Szatrowski T.P., and Nathan C.F., 1991. Production of Large Amounts of Hydrogen Peroxide by Human Tumor Cells**.** *Cancer Res*; **51**:794-798

Thomas, L., Spurlock, G., Eudall, C., Thomas, N. S., Mort, M., Hamby, S. E., Chuzhanova, N., Brems, H., Legius, E., Cooper, D. N., and Upadhyaya, M., 2011. Exploring the somatic NF1 mutational spectrum associated with NF1 cutaneous neurofibromas. *Eur J Hum Genet*; **20(4)**:411-9

Telang S., Yalcin A., Clem A.L., Bucala R., Lane A.N., Eaton J.W., and Chesney J., 2006. *Ras* Transformation requires metabolic control by 6-phosphofructo-2-kinase. *Oncogene*; **25**:7225–7234

Telang S., Lane A.N., Nelson K.K., Arumugam S., Chesney J., 2007. The oncoprotein H-RasV12 increases mitochondrial metabolism. *Molecular Cancer*. **6**:77

Tidyman, W. E., and Rauen, K. A., 2009. The RASopathies: developmental syndromes of Ras/MAPK pathway dysregulation. *Curr Opin Genet Dev;* **19**:230-236

Tong X., Zhao F., Mancuso A., Gruber J.J., and Thompson C.B., 2009. The glucose-responsive transcription factor ChREBP contributes to glucose-dependent anabolic synthesis and cell proliferation. *PNAS*; **106(51):**21660-21665

Tonsgard J.H., Kwak S.M., Short M.P., Dachman A.H., 1998. CT imaging in adults with neurofibromatosis-1: frequent asymptomatic plexiform lesions. *Neurology*; **50(6)**:1755-60

Wallace D.C., 2012. Mitochondria and cancer. *Nature Reviews Cancer*; **12(10)**:685-698

Wang, P., Song, M., Zeng, Z., Zhu, C., Lu, W., Yang, J., Ma, M., Huang, A., Hu, Y., and Huang, P. (2015). Identification of NDUFAF1 in mediating K-Ras induced mitochondrial dysfunction by a proteomic screening approach. *Oncotarget,* ***6*****(6)**:3947-3962

Warbey V., Ferner R.E., Dunn J.T., Calonje, E., O'Doherty M.J., 2009. [18F]FDG PET/CT in the diagnosis of malignant peripheral nerve sheath tumours in neurofibromatosis type-1. *European Journal of Nuclear Medicine and Molecular Imaging*; **36(5)**:751-757

Warburg O., 1956. On the Origin of Cancer Cells. *Science*; **24**: 309-314

Weinberg F., Hamanaka R., Wheaton W.W., Weinberg S., Joseph J., Lopez M., Kalyanaraman B., Mutlu G.M., Budinger G.R.S. and Chandel N.S., 2010. Mitochondrial metabolism and ROS generation are essential for Kras-mediated tumorigenicity. *PNAS*; **107(19)**:8788-8793

Wellen K.E., Thompson C.B., 2010. Cellular metabolic stress: Considering how cells respond to nutrient excess. *Molecular Cell*; **40(2)**:323-332.

Wu J., Patmore D.M., Jousma E., Eaves D.W., Breving K., Patel A.V., Schwartz E.B., Fuchs J.R., Cripe T.P., Stemmer-Rachamimov A.O., Rater N., 2014. EGFR-STAT3 signaling promotes formation of malignant peripheral nerve sheath tumors. *Oncogene*; **33(2)**:173-180.

Xu G., Lin B., Tanaka K., Dunn D., Wood D., Gesteland R., White R., Weiss R., Tamanoi R.,1990. The catalytic domain of the neurofibromatosis type 1 gene product stimulates ras GTPase and complements ira mutants of S. cerevisiae, *Cell*; **63(4)**:835-841

Yalcin A., Telang S., Clem B., Chesney J., 2009. Regulation of glucose metabolism by 6-phosphofructo-2-kinase/fructose-2,6-bisphosphatases in cancer, *Experimental and Molecular Pathology*; **86(3)**:174-179

Yang D., Wang M-T., Tang Y., Chen Y., Jiang H., Jones T.T., Rao K., Brewer G.J., Singh K.K., Nie D., 2010. Impairment of mitochondrial respiration in mouse fibroblasts by oncogenic H-RASQ6IL. *Cancer Biology & Therapy*; **9(2)**:122-133.

Yang J., Ylipää A,, Sun Y., Zheng H., Chen K., Nykter M., Trent J., Ratner N., Lev D.C., Zhang W., 2011. Genomic and Molecular Characterization of Malignant Peripheral Nerve Sheath Tumor Identifies the IGF1R Pathway as a Primary Target for Treatment. *Clinical Cancer Research;* **17(24)**:7563-7573

Zenker, M., 2011. Clinical manifestations of mutations in RAS and related intracellular signal transduction factors. *Curr Opin Pediatr*; **23**:443-451.

Zhang Y., Yang J-M., 2013. Altered energy metabolism in cancer: A unique opportunity for therapeutic intervention. *Cancer Biology & Therapy*; **14(2)**: 81-89.

Zheng H., Chang L., Patel N., Yang J., Lowe L., Burns D.K., Zhu Y., 2008. Induction of Abnormal Proliferation by Nonmyelinating Schwann Cells Triggers Neurofibroma Formation. *Cancer Cell*; **13(2)**:117-128.

Zhu J., Wang K.Z., Chu C.T., 2013. After the banquet: Mitochondrial biogenesis, mitophagy, and cell survival. *Autophagy*; **9(11)**:1663-1676